

## **Quantum Yields of CHDO above 300 nm**

Ernst-Peter Röth<sup>1</sup>, Luc Vereecken<sup>2</sup>

<sup>1</sup>Institute for Energy and Climate Research IEK-7: Stratosphere, Forschungszentrum Jülich GmbH, 52425 Jülich, Germany

<sup>2</sup>Institute for Energy and Climate Research IEK-8: Troposphere, Forschungszentrum Jülich GmbH, 52425 Jülich, Germany

Corresponding author : Ernst-Peter Röth     [e.p.roeth@fz-juelich.de](mailto:e.p.roeth@fz-juelich.de)

**Abstract :** *The photolysis of mono-deuterated formaldehyde, CHDO, is a critical process in the deuterium-enrichment of stratospheric hydrogen formed from methane. In this work, a consistent description of the quantum yields of the molecular and radical channels of the CHDO photolysis is deduced from literature data. The fluorescence measurements of Miller and Lee (1978) provided a first data set to deduce the product quantum yields. An alternative analysis is based on the measured quantum yield spectrum for the radical channel of the CD<sub>2</sub>O photolysis by McQuigg and Calvert (1969), which is corrected for wavelength dependency and combined with the CH<sub>2</sub>O quantum yield spectrum to provide an approximation for CHDO. Both approaches provide consistent results. Finally, the findings of Troe (1984, 2007) enable the specification of the pressure dependence of the quantum yield for CH<sub>2</sub>O and CD<sub>2</sub>O and, hence, for CHDO. We find that the radical channel does not show a pressure dependence, whereas the molecular channel is dominated by tunneling and quenching processes. Simplified representations are given that are readily implemented in kinetic atmospheric models. As an example of their application, the altitude dependence of the ratio of  $J(\text{CHDO} \rightarrow \text{HD} + \text{CO})$  and  $J(\text{CH}_2\text{O} \rightarrow \text{H}_2 + \text{CO})$  is provided. Also, the importance of the photolysis of formaldehyde in the atmosphere is presenting the altitudinal dependence of the isotopic fractionation through the yield of the HD channel.*

## 1 **1. Introduction**

2

3 Measurements over the last decades showed that molecular hydrogen, H<sub>2</sub>, in the stratosphere  
4 is enriched in deuterium compared to H<sub>2</sub> in the troposphere (see e.g.: Ehhalt and Volz, 1976;  
5 Gerst and Quay, 2001; Rahn et al., 2003; Rice et al., 2003; Röckmann et al., 2003; McCarthy  
6 et al., 2004; Rhee et al., 2006). Gerst and Quay (2001) suggested that this enrichment could be  
7 due to the differential isotope fractionation in the photo-oxidation of methane. Measurements  
8 of the vertical profiles of the isotope content in H<sub>2</sub> and CH<sub>4</sub>, available since 2003, allowed the  
9 interpretation and modeling of the observed enrichment (see e.g. Pieterse et al., 2011). The  
10 methane photo-oxidation consists of various reaction steps, each of which contribute kinetic  
11 isotope effects, KIE, that have to be considered (e.g. Feilberg et al., 2005; Mar et al., 2007).  
12 The last but critical step in the reaction chain to produce the hydrogen isotope HD from the  
13 mono-deuterated isotopologue of formaldehyde, CHDO, is its photolysis.

14

15 Compared to CH<sub>2</sub>O, the available data for the mono-deuterated isotopologue CHDO are  
16 scarce. Only its spectrum was measured (c.f. Mainz Spectral Atlas, Keller-Rudek and  
17 Moortgat, 2021). The quantum yields for the molecular and the radical fragmentation  
18 branches of the CHDO photolysis, as well as the rate constants for the quenching reactions  
19 were not measured at all or with insufficient accuracy. Thus, despite its importance for the  
20 atmospheric production of HD, the photolysis of CHDO is still poorly defined; at this time, it  
21 is the most uncertain factor in the overall fractionation of formaldehyde. For example, the  
22 measured or estimated fractionation factors for the molecular channel range from 1.08 to 1.82  
23 (e.g. Feilberg et al., 2005; Rhee et al., 2006, Mar et al., 2007; Nilsson et al., 2009; Röckmann  
24 et al., 2010). Moreover, the measurements by Nilsson et al. (2009) are the only ones  
25 considering the pressure dependence of the fractionation factor due to reactions R3, R4, and  
26 R7 (see Table 1).

27

28 In this work, we aim to provide information for the modeling of CHDO photochemistry for  
29 atmospheric conditions, i.e. for a limited domain of temperature and pressure, by deducing the  
30 molecular and radical quantum yields  $\Phi^{\text{mol}}$  and  $\Phi^{\text{rad}}$  for CHDO from literature information,  
31 based on the scant data available and supplemented by a number of plausible assumptions.  
32 We do this based on two approaches: the first is based on the fluorescence measurements of  
33 Miller and Lee (1978) and literature data on energy transitions (e.g. Yeung and Moore, 1973;  
34 Chuang et al., 1987; Osborn, 2008; Fu et al. 2011). The second approach assumes that the

35 measurements of McQuigg and Calvert (1969) can be corrected via the comparison of the  
 36 CH<sub>2</sub>O measurement with later experiments (see e.g. the overview by Röth and Ehhalt, 2015).  
 37 The photochemistry derived thus is then used to assess the altitudinal dependence of the  
 38 CHDO isotopic fractionation.

39  
 40

## 41 2. Photolysis reaction mechanism

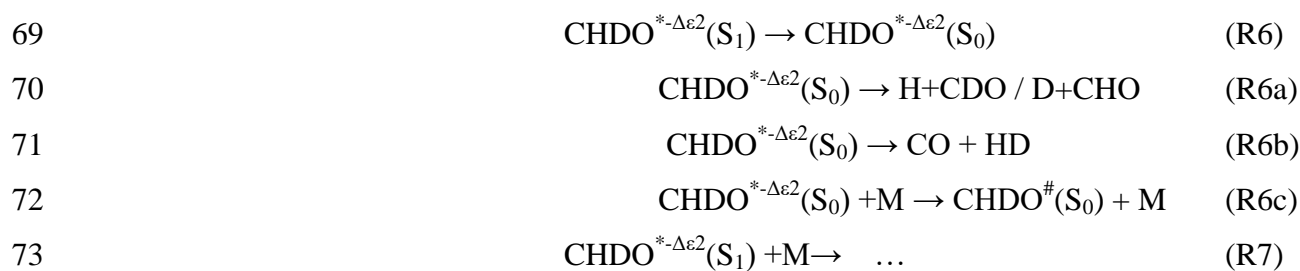
42

43 Based on the available literature (e.g.: Aràujo et al., 2009; Breuer and Lee, 1971; Chuang et  
 44 al., 1987; Yamaguchi et al., 1998) we propose a photolytic reaction scheme of CHDO in  
 45 Table 1, analogous to that of CH<sub>2</sub>O (Röth and Ehhalt, 2015). The scheme involves a  
 46 cascading series of fragmentation channels competing with stepwise quenching by collisional  
 47 energy loss, starting at the excited singlet state S<sub>1</sub>. Reactions via the triplet state of CHDO are  
 48 not considered here, as they are only accessible at wavelengths below 300 nm (Aràujo et  
 49 al.,2009), while we concentrate on wavelengths above this limit in this work. Under  
 50 atmospheric conditions, which are considered here, the system is thermalized.

51

52 **Table 1** : Reaction scheme of the photolysis of CHDO occurring over the S<sub>1</sub> and S<sub>0</sub> electronic  
 53 singlet states.  $-\Delta\epsilon_1$ ,  $-\Delta\epsilon_2$  indicate the collisional energy losses to bath gas M in the respective  
 54 reactions. This quenching is stepwise but is represented here for energies above/below the  
 55 threshold for dissociation; the asterix \* stands for excitations able to lead to bond breaking,  
 56 whereas the index # indicates lower energies and lead ultimately to thermalized CHDO.





75 After excitation of the ground state  $\text{CHDO}(\text{S}_0)$  (R0) by a photon of a given wavelength, the  
 76 excited reaction product  $\text{CHDO}^*(\text{S}_1)$  decays by fluorescence (R1), or transitions to the  $\text{S}_0$   
 77 ground state surface as an excited  $\text{CHDO}^*$  molecule with either all available energy (R2) or  
 78 with a variable amount of energy  $-\Delta\epsilon_1$  lost by quenching (R3). These excited  $\text{CHDO}^*(\text{S}_0)$  and  
 79  $\text{CHDO}^{*\Delta\epsilon_1}(\text{S}_0)$  can in turn be quenched by the bath gas in a cascading series (R2c, R3c, R6c),  
 80 at each energy level competing with fragmentation to radicals  $\text{H+CDO/D+CHO}$  (R2a,  
 81 R3a,R6a) or to molecular products  $\text{CO+HD}$  (R2b, R3b,R6b), as described for  $\text{CH}_2\text{O}$  by  
 82 Yeung and Moore, (1973). Alternatively, the excited  $\text{CHDO}^*(\text{S}_1)$  can lose an amount of  
 83 energy by quenching, but remain on the  $\text{S}_1$  excited electronic surface (R4). This state can then  
 84 undergo processes as above, i.e. decay by fluorescence (R5), transition to the  $\text{S}_0$  ground state  
 85 without (R6) or with (R7) energy loss by quenching, where once again it can undergo further  
 86 quenching (R6c) in competition with fragmentation (R6a, R6b). Overall, this scheme  
 87 represents a cascading series of quenching steps competing against decomposition and  
 88 fluorescence. Only the first few steps in the cascade are represented, but more cascading steps  
 89 are possible at lower internal energies. According to the analysis of the fluorescence  
 90 measurements by Miller and Lee (1978), these lower-energy reactions are not critical and  
 91 need not be considered in detail. Here, R7 simply represents the summation of all subsequent  
 92 cascades, from which negligible channels such as *e.g.* the fluorescence channels are omitted.  
 93 Schematic energy diagrams for this reaction mechanism were already depicted in the  
 94 literature (*e.g.* Fig.3 in Araújo et al., 2009 and Fig.1 in Chuang et al., 1987), and are not  
 95 repeated here.

96

97 The quantum yield  $\Phi^{\text{rad}}$  represents the combined fragmentation to radicals (R2a, R3a, R6a),  
 98 while summed fragmentation through the molecular branches (R2b, R3b, R6b) is described by  
 99 the quantum yield  $\Phi^{\text{mol}}$ . The total photolysis quantum yield  $\Phi^{\text{tot}}$ , i.e. the decay of excited  
 100 formaldehyde into products other than its ground-state, can be experimentally derived from  
 101 the observed CO production, where CDO and CHO radical fragments react with  $\text{O}_2$  to form

102 CO and HO<sub>2</sub> / DO<sub>2</sub>. The quantum yield of the fluorescence is always less than 1% (Miller  
103 and Lee, 1978) and is omitted henceforth.

$$104 \quad \Phi^{tot} = \Phi^{mol} + \Phi^{rad} \quad (F1)$$

105 Obviously, the sum of  $\Phi^{tot}$  and  $\Phi^{quench}$ , the summed yield of the quenching reactions (R2c,  
106 R3c, R6c), must equal 1 at any wavelength  $h\nu$ .

$$107 \quad \Phi^{tot} + \Phi^{quench} = 1 \quad (F2)$$

108  
109

### 110 3. Analysis of fluorescence measurements

111

112 From the fluorescence measurements of Miller and Lee (1978) the quantum yields of both the  
113 fluorescence and the total non-CHDO products can be derived. The contribution of the second  
114 step in the reaction cascade is small at low pressure (see later), so we assume that Table X  
115 provided by these authors directly gives the reaction rate constants  $k_1$  and  $k_2$ , where  $k_1$  equals  
116 the reciprocal lifetime  $\tau_{radiation}$  listed and  $1/k_2$  is the non-radiative lifetime. Similarly, the  
117 constants  $k_5$  and  $k_6$  are determined by the lifetimes of the next lower vibrational level.

118

119 The reaction constants  $k_3$ ,  $k_4$ , and  $k_7$  can be deduced from the pressure dependence of the  
120 CHDO fluorescence quantum yield in the Table II of Miller and Lee (1978). In the present  
121 paper only the quantum yields at pressures above 1 Torr are considered, where the Ar bathgas  
122 used is assumed to have similar collisional properties as air (Hirschfelder et al., 1954). For  
123 each wavelength the pressure dependence of the data is fitted by a Simplex algorithm  
124 according to Nelder and Mead (1965) by formula F3 for the fluorescence quantum yield  $\Phi_F$ .

$$125 \quad \Phi_F(M) = \frac{k_1}{\alpha} + \frac{k_4[M] \cdot k_5}{\alpha \cdot \beta} \quad (F3)$$

126 with  $\alpha = k_1 + k_2 + k_3[M] + k_4[M]$  and  $\beta = k_5 + k_6 + k_7[M]$ . For consistency we only used  
127 the  $2^i 4^j$  transitions, only.

128

129 The corresponding reaction constants are listed in Table 2. With this data set the experimental  
130 fluorescence measurements are well fitted as shown in Figure 1 where, to improve the clarity  
131 of the fit, only the pressure dependent part  $\theta(M)$  of equation F3 is plotted vs pressure:

$$132 \quad \theta(M) = \frac{k_1}{\Phi_F(M)} - (k_1 + k_2) \quad (F4)$$

133

134 **Table 2** : Results of the least square fit of the quantum yields of CHDO (Miller and Lee  
 135 (1978).  $k_1$ ,  $k_2$  and  $k_5$ ,  $k_6$  are literature data (Miller and Lee, 1978),  $k_3$ ,  $k_4$ , and  $k_7$  are deduced  
 136 from these data.

Wavelength [nm]	$k_1$ [ $10^5 \text{s}^{-1}$ ]	$k_2$ [ $10^8 \text{s}^{-1}$ ]	$k_3$ [ $10^{-11} \text{cm}^3 \text{s}^{-1}$ ]	$k_4$ [ $10^{-11} \text{cm}^3 \text{s}^{-1}$ ]	$k_5$ [ $10^5 \text{s}^{-1}$ ]	$k_6$ [ $10^8 \text{s}^{-1}$ ]	$k_7$ [ $10^{-12} \text{cm}^3 \text{s}^{-1}$ ]
314.0	3.03	1.79	29.7	4.59	2.78	0.50	0.57
318.3	2.50	1.32	15.4	3.48	2.50	0.40	1.15
325.7	2.78	0.50	10.9	1.77	3.57	0.22	1.79
330.8	2.50	0.40	4.81	1.05	2.44	0.13	1.35
338.6	3.57	0.22	4.89	0.84	3.45	0.07	0.77
344.4	2.44	0.13	5.95	2.78	2.40*	0.06*	1.39
352.9	3.45	0.07	2.38	0.76	4.00*	0.03*	1.24

137 \* estimated by extrapolation of the other values

138  
 139 The energy transferred in reaction R2 is either quenched to form a stable molecule  
 140 CHDO<sup>#</sup>(S<sub>0</sub>) or used to drive fragmentation to molecular (CO + HD) or radical products  
 141 (H+CDO / D+CHO). Hence, the reactions R2a and R2b form part of the product-forming  
 142 channel. Analogously, the secondary reactions of the pressure dependent reactions R3 and R4  
 143 lead to products via the reactions R3a and R3b, respective R6a and R6b. With this, the total  
 144 product quantum yield of the photolysis of CHDO is the sum of the individual product  
 145 quantum yields across all channels k, where the index k=2, 3, 6 stands for the non-radiative  
 146 reactions R2, R3, and R6.

147 The individual product quantum yield can be approximated by

$$148 \quad \Phi_k^{tot} = \frac{1}{1+a \cdot \exp\left(\frac{\varepsilon_k - \varepsilon_0}{b}\right) \cdot \frac{[M]}{[M_0]}} \quad (\text{F5})$$

149 analog to the publication by Röth and Ehhalt (2015) on CH<sub>2</sub>O.

150 In equation F5,  $\varepsilon_2$  is the excitation energy of the photolysis reaction. The energies  $\varepsilon_3$  and  $\varepsilon_6$   
 151 are related to  $\varepsilon_2$  by the approximated energy transfer in a collision, respective by the averaged  
 152 width of the band intervals, given by  $\varepsilon_3 = \varepsilon_2 - 0.0124 \text{ eV}$  (Troe, 2007) and  $\varepsilon_6 = \varepsilon_2 - 0.13 \text{ eV}$   
 153 (Miller and Lee, 1978). The pivot wavelength  $1/\varepsilon_0$  is 348.6 nm, as published in Nilsson et al.  
 154 (2014) from quantum chemical calculations of the barriers to dissociation of H-CHO, H-  
 155 CDO, D-CHO, and D-CDO.

156  
 157 The total quantum yield of the products (molecules plus radicals) can be deduced from the  
 158 rate constants of Table 2 and the measurements of Nilsson et al. (2010, 2014), who

159 investigated the pressure dependence of the kinetic isotope effect KIE of the photolysis  
 160 frequencies of CH<sub>2</sub>O and CHDO.

$$161 \quad KIE = \frac{j_{CH_2O}}{j_{CHDO}} \quad \text{with} \quad j = \int \Phi_{CH_2O/CHDO}^{tot} \sigma F d\lambda \quad (F6)$$

162 As the quantum yield of CH<sub>2</sub>O is known from the literature (see e.g. Röth and Ehhalt, 2015)  
 163  $\Phi_{CHDO}^{tot}$  remains the only unknown factor in formula F6. With the actinic flux density F of the  
 164 lamp used by Nilsson et al. (2014) and the absorption spectra  $\sigma_x$  of CH<sub>2</sub>O and CHDO from  
 165 Gratien et al. (2007) the ratio KIE can be calculated with optimized values for  $a$  and  $b$  in eq.  
 166 F5. Comparing the results of the simulation with the measured data by Nilsson et al. (2010,  
 167 2014) the constants  $a$  and  $b$  can be determined via a least square fit. Figure 2 presents the  
 168 result with optimized values  $a=2.94$  and  $b=6.5 \times 10^{-5} \text{ nm}^{-1}$  together with the measurements.  
 169 The data at 1000 hPa is included in the fit as its mean value to accommodate the large  
 170 variation of the data.

171

172 The total product quantum yield, deduced from the reaction scheme R0 to R7 is

$$173 \quad \Phi^{tot} = \frac{k_2}{\alpha} \cdot \Phi_2^{tot} + \frac{k_3[M]}{\alpha} \cdot \Phi_3^{tot} + \frac{k_4[M]}{\alpha} \cdot \frac{k_6}{\beta} \cdot \Phi_6^{tot} \quad (F7)$$

174 with  $\alpha$  and  $\beta$  as defined in formula F3, and  $\Phi_k^{tot}$ , the sub-product yield, according to formula  
 175 F5. The measured wavelength dependence of  $\Phi^{tot}$  at 1000 hPa pressure is depicted in Figure 3,  
 176 where the total quantum yield is calculated with the rate constants from Table 2. The pressure  
 177 dependence of the three terms of  $\Phi^{tot}$  is illustrated in Figure 4.

178

179 To obtain a continuous and smooth wavelength dependence, the rate constants  $k_1$  through  $k_7$   
 180 can be represented by an approximation function

$$181 \quad k = A \exp(B(\lambda - 300 \text{nm})) \quad (F8)$$

182 The values for the parameters A and B are obtained from a least square fit to the data in Table  
 183 2 and listed in Table 3. Where-ever the value of B was less than 0.001 it was set to 0, and A  
 184 then corresponds directly to the mean of the respective rate constant. The wavelength  
 185 dependence of  $\Phi^{tot}$  at 1000 hPa with these functions is presented by the solid line in Figure 3.  
 186 The comparison to the experimental data by Miller and Lee (1978) suggests a variance of the  
 187 data of around 15%.

188

189 **Table 3:** Parameters of the rate constants according to equation F8, B in  $\text{nm}^{-1}$  and A in  $\text{s}^{-1}$ ,  
 190 respective in  $\text{cm}^3 \text{s}^{-1}$ , derived from least square fits.

	$k_1$	$k_2$	$k_3$	$k_4$	$k_5$	$k_6$	$k_7$

<b>A</b>	$2.90 \times 10^5$	$6.10 \times 10^8$	$7.70 \times 10^{-10}$	$1.30 \times 10^{-10}$	$3.00 \times 10^5$	$1.50 \times 10^8$	$1.2 \times 10^{-12}$
<b>B</b>	0	0.086	0.069	0.071	0	0.075	0

191

192 For CHDO the only quantitative indication for the quantum yield of the radical channel in the  
 193 literature are measurements of the kinetic isotope effect KIE (Feilberg et al., 2007, Rhee et al.,  
 194 2008, Röckmann et al., 2010, and Nilsson et al., 2014). Following eq. F5, simulating these  
 195 KIE-measurements requires three parameters for the individual radical quantum yield  
 196  $\Phi_k^{rad}$  expressed in eq. F9: the maximum value  $\Phi^{max}$  of the wavelength dependence, its  
 197 curvature  $b$ , and the pivot wavelength  $\lambda_0$ . The parameter  $a$  is set to 1, as for the radical  
 198 quantum yield no pressure dependence is assumed, cancelling the  $[M]/[M_0]$  factor.

$$199 \quad \Phi_k^{rad} = \frac{\Phi^{max}}{1 + a \exp\left(\frac{\epsilon_k - \epsilon_0}{b}\right)} \quad (F9)$$

200 Analog to the analysis for CH<sub>2</sub>O (Röth and Ehhalt, 2015), where the curvatures of the  
 201 wavelength dependence of  $\Phi^{tot}$  and  $\Phi^{rad}$  are similar,  $b$  can be set to  $6.5 \times 10^{-5} \text{ nm}^{-1}$  for the  
 202 radical quantum yield of CHDO. The maximum  $\Phi^{max}$  was varied in the interval [0.70 / 0.78]  
 203 around the corresponding value for CH<sub>2</sub>O, but the resulting scattering is very small (see  
 204 shaded area in Fig. 5). Consequently, parameter  $\Phi^{max}$  is set to 0.74, matching the value also  
 205 used for CH<sub>2</sub>O (Ehhalt and Röth, 2015).

206

207 With these parameters the KIE of 1.63 as measured by Röckmann et al. (2010) was fitted with  
 208 the actinic flux density given by Röckmann et al. and the optical spectra by Gratien et al.  
 209 (2007). The best fit gave a pivot wavelength  $\lambda_0$  of 327 nm. This value lies in the middle of the  
 210 bond energies of 362.63 kJ/mol for C-H and 369.6 kJ/mol for C-D, calculated by Chuang et  
 211 al. (1987). With the constants  $\Phi^{max} = 0.74$ ,  $a=1$ ,  $b = 6.5 \cdot 10^{-5} \text{ nm}^{-1}$  and  $1/\epsilon_0 = 327.1 \text{ nm}$  the  
 212 quantum yield function  $\Phi^{rad}$  of the radical channel of CHDO is analog to F7:

$$213 \quad \Phi^{rad} = \frac{k_2}{\alpha} \cdot \Phi_2^{rad} + \frac{k_3[M]}{\alpha} \cdot \Phi_3^{rad} + \frac{k_4[M]}{\alpha} \frac{k_6}{\beta} \cdot \Phi_6^{rad} \quad (F10)$$

214 where the radical quantum yields of the individual channels is given by function F9 and with  
 215  $\alpha$  and  $\beta$  as defined in F3. Figure 5 depicts the wavelength dependence of the total quantum  
 216 yield together with that for the radicals. At atmospheric pressures, as considered in this paper,  
 217 the contributions of the individual quenching processes are insignificant with respect to the  
 218 overall radical quantum yield.

219

220 To provide a more handy tool for atmospheric modeling, we introduce an exponential  
 221 function (F11), with only one term and three parameters for the total and the radical quantum

222 yields of CHDO, similar to those deduced by Ehhalt and Röth (2015) for CH<sub>2</sub>O, as a proxy  
 223 for the three-term functions F7 and F10:

$$224 \quad \Phi = \frac{a}{1 + \exp\left(\frac{-\left(\frac{1}{\lambda} - \frac{1}{\lambda_0}\right)}{b}\right) \frac{[M]}{[M_0]}} \quad (\text{F11})$$

225 The corresponding parameters for the total quantum yield of CHDO are  $a=1.0$ ,  $b=7.7 \times 10^{-5} \text{ s}^{-1}$ ,  
 226 and  $\lambda_0=336.2 \text{ nm}$ . For the radical channel the factor  $[M]/[M_0]$  is set to 1, as the photolysis  
 227 leading to the radicals is nearly pressure independent. The respective parameters are  $a=0.74$ ,  
 228  $b=7.7 \times 10^{-5} \text{ s}^{-1}$ , and  $\lambda_0=325.0 \text{ nm}$ . Both approximation curves are depicted in Figure 5, and  
 229 Figure 6 shows the pressure dependent comparison with the measured data by Miller and Lee  
 230 (1978).

231

232

#### 233 **4. Analysis of the CHDO photo-decomposition**

234 Our second approach to estimate the quantum yields for the photolysis of CHDO is based on  
 235 the experiments of McQuigg and Calvert (1969) who measured the photo-decomposition of  
 236 CH<sub>2</sub>O, CHDO, and CD<sub>2</sub>O. Unfortunately, the authors only presented the quantum yields for  
 237 the two radical reaction channels of CH<sub>2</sub>O and CD<sub>2</sub>O. They further assumed that the total  
 238 quantum yield equals 1, independent of wavelength. It appears, however, that these data have  
 239 a bias which becomes evident when the data for CH<sub>2</sub>O are compared to more recent  
 240 measurements.

241

242 In Figure 7 the dependence on the wavelength of  $\Phi^{\text{rad}}$  of CH<sub>2</sub>O by McQuigg and Calvert  
 243 (1969) is depicted together with a curve for CH<sub>2</sub>O, averaged over measured data from the  
 244 paper by Röth and Ehhalt (2015). The latter evaluation showed no pressure dependence, but  
 245 indicated a weak temperature effect which is neglected here. The curve is represented by the  
 246 following function:

247

$$248 \quad \Phi_{\text{CH}_2\text{O}}^{\text{rad}} = \frac{0.74}{1 + \exp\left(\frac{-\left(\frac{1}{\lambda} - \frac{1}{327.4}\right)}{5.4 \times 10^{-5}}\right)} - \frac{0.40}{1 + \exp\left(\frac{\frac{1}{\lambda} - \frac{1}{279.0}}{5.2 \times 10^{-5}}\right)} \quad (\text{F12})$$

249 Equation F12 exhibits a maximum in  $\Phi^{\text{rad}}$  around 310 nm, independent of the small  
 250 temperature shift, whereas the earlier values of McQuigg and Calvert exhibit a monotonic  
 251 decay with increasing wavelength above 280 nm, which points to a bias in the latter. The  
 252 second summand in F12 is less than 1% at wavelengths above 300 nm and, hence, can be

253 omitted in the present paper. Figure 7 also includes the data of McQuigg and Calvert (1969)  
 254 for CD<sub>2</sub>O which show a quite similar wavelength dependency as the data for CH<sub>2</sub>O.

255

256 Our first assumption is that the bias in the experiments of McQuigg and Calvert extends  
 257 equally to both isotopologues (CD<sub>2</sub>O and CH<sub>2</sub>O), and that, therefore, the ratio R of their  
 258 quantum yields is correct. This ratio is displayed in Figure 8 and shows a mostly monotonic  
 259 decrease with increasing wavelength. In this context, it is interesting to note that the ratio of  
 260 the rate constants for the decomposition of excited CH<sub>2</sub>O\* and CD<sub>2</sub>O\* into the respective  
 261 radical channels, as calculated by Troe (1984) from theory, result in a curve with a monotonic  
 262 decrease with increasing wavelength similar to that of the quantum yield ratio (see Figure 8).

263 Using ratio R together with the fit function F12 for  $\Phi_{CH_2O}^{rad}$  allows to estimate  $\Phi_{CD_2O}^{rad}$  for the  
 264 radical channel of CD<sub>2</sub>O, as shown in Figure 8.

265 To calculate  $\Phi_{CHDO}^{rad}$  we need one further assumption. Our hypothesis is suggested by the  
 266 results of Feilberg et al. (2004), who found that the KIE of the reactions of CHDO with OH,  
 267 Cl and Br are arithmetic means of the KIE of the reactions of CH<sub>2</sub>O and CD<sub>2</sub>O with those  
 268 radicals. This in turn implies that the C-H bond strengths are similar in the isotopologues, and  
 269 the same is true for the C-D bond strength. We, therefore, assume that  $\Phi_{CHDO}^{rad}$  can be  
 270 calculated from the average of  $\Phi_{CH_2O}^{rad}$  and  $\Phi_{CD_2O}^{rad}$  at each wavelength:

$$271 \quad \Phi_{CHDO}^{rad}(\lambda) = \left( \Phi_{CH_2O}^{rad}(\lambda) + \Phi_{CD_2O}^{rad}(\lambda) \right) / 2 \quad (F13)$$

272 The resulting radical quantum yields are compared in Figure 9.  $\Phi_{CHDO}^{rad}$  does not depend on  
 273 pressure since neither  $\Phi_{CH_2O}^{rad}$  nor  $\Phi_{CD_2O}^{rad}$  are pressure dependent. The respective maxima in  
 274  $\Phi^{rad}$ , on the other hand, decrease from 0.72 over 0.70 to 0.65 for increasing deuteration.

275 Moreover, there is a blue shift of 5 nm, resp. 10 nm in the decreasing part of the quantum  
 276 yield spectra of CHDO and CD<sub>2</sub>O, i.e. at wavelengths above 315 nm. These blue shifts have  
 277 the same tendency but do not quite match the measured threshold energies of 362.3 kJ/mol,  
 278 368.4 kJ/mol, and 370.6 kJ/mol for CH<sub>2</sub>O, CHDO, and CD<sub>2</sub>O, respectively (Chuang et  
 279 al.,1987), which correspond to the wavelengths 330.9 nm, 325.5 nm, and 323.5 nm.

280

281 The one-term fit function for the radical channel of CHDO is:

$$282 \quad \Phi_{CHDO}^{rad} = \frac{0.72}{1 + \exp\left(\frac{-\left(\frac{1}{\lambda} - \frac{1}{323.0}\right)}{7.7 \times 10^{-5}}\right)} \quad (F14)$$

283 and is also show in Figure 9. In Figure 10 the result of the interpretation of the measured  
 284 photo-decomposition of CHDO by McQuigg and Calvert (1969) is compared to the radical

285 quantum yield deduced from the fluorescence measurements of Miller and Lee (1978). Both  
 286 estimations lead to a wavelength dependence of  $\Phi_{CHDO}^{rad}$  which lie in each others uncertainty  
 287 range. This is a strong hint that the deduced results are robust and represent the true quantum  
 288 yield of the radical channel of the photolysis of CHDO.

289  
 290

## 291 **5. The isotope fractionation during the photolysis of formaldehyde**

292

293 The photolysis frequency  $J_i$  of the isotopologues  $CH_2O$  and  $CHDO$  is given by the integration  
 294 of quantum yield  $\Phi$ , absorption cross section  $\sigma$ , and spectral actinic photon flux density  $F_\lambda(\lambda)$   
 295 over the  $\lambda$  wavelength domain:

$$296 \quad J_i = \int \Phi_{i,j}(\lambda) \cdot \sigma_i(\lambda) \cdot F_\lambda(\lambda) d\lambda \quad (F15)$$

297 where the quantum yield  $\Phi_{i,j}(\lambda)$  depends on the product channel  $j$ , either molecular or radical,  
 298 of isotopologue  $i$ , and the absorption cross section  $\sigma_i(\lambda)$  is specific to the isotopologues  $i$ . For  
 299 our calculations the absorption spectra of  $CH_2O$  and  $CHDO$  from Gratien et al. (2007) were  
 300 applied. We used these values instead of the JPL-recommendation (Burkholder, 2020) for  
 301 consistency with the calculations in section 2 and 3. The solar spectral actinic flux density  $F_\lambda$   
 302 was calculated from a quasi-spherical 1-D radiation transfer model (Röth, 2002); the  $\Phi(\lambda)$  are  
 303 those from section 2. An example of the terms  $\Phi^{mol}(\lambda)$ ,  $\sigma(\lambda)$ ,  $F_\lambda(\lambda)$  for the molecular channel  
 304 of  $CHDO$  is given in Figure 11 for the pressure and temperature at an altitude of 20 km. The  
 305 product of these terms, integrated over 5 nm intervals for better visibility, is also displayed to  
 306 demonstrate the spectrally resolved contributions to the photolysis frequency of the molecular  
 307 channel of  $CHDO$ .

308

309 The kinetic isotope effect for the molecular channel is given by

$$310 \quad KIE_{mol} = \frac{J_{CH_2O}^{mol}}{J_{CHDO}^{mol}} \quad (F16)$$

311 and correspondingly for the radical channel

$$312 \quad KIE_{rad} = \frac{J_{CH_2O}^{rad}}{J_{CHDO}^{rad}} \quad (F17)$$

313 For a quick overview the dependence of  $KIE_{rad}$  and  $KIE_{mol}$  on altitude for globally averaged  
 314 conditions (equinox, 30°N) are depicted in Figures 12a and 12b.  $KIE_{mol}$  decreases  
 315 monotonically with decreasing pressure from 1.59 at 1000 hPa to 1.06 at 1 hPa. The radical  
 316 channel in contrast shows hardly any pressure dependency as the rate of this reaction is not  
 317 influenced by the quenching process. The marginal variation of the kinetic isotope effect with

318 altitude is caused by the altitudinal increase of the photon flux and its differing contribution to  
319 the photolysis frequency integrals of CH<sub>2</sub>O and CHDO.

320

321 To examine whether the quantum yield functions for CHDO deduced above are applicable for  
322 modeling purposes, additional sensitivity studies were carried out, varying the main features  
323 of the quantum yield functions. With respect to the fractionation factor, only the variations of  
324 those parameters are relevant which alter the relation of the entire photolysis frequency  
325 integrals (eq. F15) of the molecular and the radical channels. In Figures 12a and 12b we  
326 additionally show the variances of the photolysis frequencies as well as of the fractionation  
327 factors. The shaded area is produced by varying one parameter of the CHDO quantum yield  
328 as indicated below. The photolysis frequency of CH<sub>2</sub>O remained unchanged.

329

330 The sensitivity of the molecular branch of the photolysis frequency of CHDO to the  
331 preexponential factor of the quantum yield function is roughly 10 % throughout the  
332 atmosphere if this value is varied by 10%. All other parameters do not alter the integral  
333 equation F15 significantly and produce only variances less than 1 % when changed by 10%. It  
334 can thus be concluded that the estimated equation parameters are good representations of the  
335 actual values. At higher altitudes (<10 hPa)  $\Phi_{CHDO}^{mol}$  and  $\Phi_{CH_2O}^{mol}$  are close to unity in the  
336 wavelength regime 330 nm to 360 nm (see e.g. Fig. 6). So, the photolysis frequency in the  
337 stratosphere does not change much if the parameters of the respective functions are varied.  
338 Therefore, the variance of the fractionation factor does not much decrease above 30 km  
339 altitude. Here, measurements at tropospheric pressures could be much more informative as  
340 becomes evident from Figure 12.

341

342 The photolysis frequency of the radical channel of CHDO is only sensitive to the maximum of  
343 the quantum yield and to the threshold wavelength 323 nm. Shifting the latter value by  $\pm 3$  nm  
344 produces changes of about 20 % in the troposphere, decreasing to 10 % at 50 km altitude as  
345 shown in Figure 12. This variation of the threshold produces an error bar of the fractionation  
346 factor of the same magnitude.

347

348

349 **6. Discussion**

350

351 Due to consecutive reactions only the molecular channel contributes to the HD production.  
352 Up to now there had been a handicap in the interpretation of stratospheric measurements of  
353 the concentration of deuterated hydrogen HD due to the lack of exact knowledge of the  
354 photolysis frequencies of deuterated formaldehyde, resulting in an uncertainty on the  
355 fractionation factor. There have been a number of experimental approaches to deduce the  
356 fractionation factor, where e.g. Feilberg et al. (2005) measured a value of  $1.82 \pm 0.07$  for  $\alpha_{\text{mol}}$ ,  
357 while Röckmann et al. (2010) found a value of  $1.63 \pm 0.03$  for that ratio. In their modeling  
358 paper, Mar et al. (2007) varied the fractionation factor between 1.2 and 1.5 for stratospheric  
359 conditions.

360

361 In all these studies the pressure dependence of the photolysis frequencies could not be  
362 investigated. An interesting experiment by Nilsson et al. (2009) addressed this problem.  
363 Unfortunately, the spectral radiance of the light source used did not resemble the sun light  
364 well enough, and their findings could not be transferred to the real atmosphere without  
365 information on the quantum yield of CHDO.

366

367 Beside its pressure dependence the variation of the photolytic fractionation factors can also be  
368 caused by different actinic fluxes at the times and sites of the experiments. The actinic flux in  
369 the numerator and denominator of the fractionation factor in equations F16 and F17 do not  
370 cancel out, and, therefore, the factor is depending on the local insolation conditions.

371 Calculations of the solar zenith angle (SZA) dependency with the complex radiation transfer  
372 model ART (Röth, 2002) result in values from 1.47 at overhead sun to 1.95 at  $\text{SZA}=83^\circ$  for  
373 clear sky and free horizon at ground level. This zenith angle dependency is less expressed at  
374 20 km altitude and disappears at 50 km, as depicted in Figure 13. This effect may explain the  
375 differences in the measurements of the fractionation factors. To check the variance with the  
376 solar zenith angle the measured fractionation factor  $\text{KIE}_m$  (eq. F16) is compared to model  
377 calculations. The factor  $1.63 \pm 0.03$  (Röckmann et al., 2010) was derived from experimental  
378 studies in the atmospheric simulation chamber SAPHIR between  $60^\circ$  and  $70^\circ$  SZA  
379 (Röckmann et al., 2010). The absorption cross sections by Gratien et al. (2007) and the  
380 quantum yields derived above together with the radiation spectra result in a fractionation  
381 factor of 1.54 for  $60^\circ$  SZA and 1.70 for  $70^\circ$  SZA are in good agreement with the measured  
382 value.

383

384 **Conclusions**

385  
386 The current work derives a framework and set of equations for describing the CHDO  
387 photolysis, based on two different approaches building on the available literature data, finding  
388 a consistent result across all data sets. It could be shown that the most influential parameters  
389 of the rates of photolysis of CHDO are the absolute value and the threshold of the quantum  
390 yield of the radical channel. Simplified parametrized equations (F11 and F14) that are readily  
391 implemented in kinetic models are provided for these quantities. Measurements around 300  
392 nm and 325 nm could help to further reduce the uncertainty on the fractionation factor.  
393 Additional measurements of the pressure dependence of the total quantum yield, i.e. the  
394 quenching rate of excited CHDO<sup>\*</sup>, would be valuable to further test the assumptions made in  
395 this paper.

396

#### 397 **Competing interests**

398 The authors declare they have no competing interests

399

400

401

#### 402 **Acknowledgments**

403 The authors thank Dr. B. Bohn and Dr. D. Tarraborrelli for their useful comments and  
404 suggestions to improve the clarity and readability of the paper.

405

406 **References**

- 407  
408 Araujo, M., Lasome, B., Magalhaes, A. L., Worth, G. A., Bearperk, M. J., and Robb, M. A.  
409 *The molecular dissociation of formaldehyde at medium photoexcitation energies: A quantum*  
410 *chemistry and direct quantum dynamics study*  
411 J. Chem. Phys. 131, 144301-1 – 144301-8, 2009  
412  
413 Breuer, G. M., and Lee, E. K. C.  
414 *Fluorescence decay times of Cyclic Ketones, Acetone, and Butanal in the gas phase*  
415 J. Phys. Chem. 75, 989 – 990, 1971  
416  
417 Burkholder, J. B., Sander, S. P., Abbatt, J. P. D., Barker, J. R., Cappa, C., Crous, D., Dipple,  
418 T. S., Huie, R. E., Kolb, C. E., Kurylo, M. J., Orkin, V. L., Percival, C. J., Wilmouth, D. M.,  
419 and Wine, P. H.  
420 *Chemical kinetics and photochemical data for use in atmospheric studies*  
421 JPL-Publication 19-5, Pasadena, 2020  
422  
423 Chuang, M-C., Foltz, M. F., and Moore, C. B.  
424 *T<sub>1</sub> barrier height, S<sub>1</sub>-T<sub>1</sub> intersystem crossing rate, and S<sub>0</sub> radical dissociation threshold for*  
425 *H<sub>2</sub>CO, D<sub>2</sub>CO, and HDCO*  
426 J. Chem. Phys. 87, 3855 – 3864. 1987  
427  
428 Ehhalt, D. H., Volz, A.  
429 *Coupling of the CH<sub>4</sub> with the H<sub>2</sub> and CO cycle : isotopic evidence*  
430 In : Symposium on Microbiol. Production and Utilization of Gases (H<sub>2</sub>, CH<sub>4</sub>, and CO)  
431 (eds.: Schlegel, H. G., Gottschalk, G., Pfenning, N.), Akad. Wiss. Göttingen, Germany, 1976  
432  
433 Feilberg, K. L., Johnson, M. S., Nielsen, C. J.  
434 *Relative Reaction Rates of HCHO, HCDO, DCDO, H<sup>13</sup>CHO, and HCH<sup>18</sup>O with OH, Cl, Br,*  
435 *and NO<sub>3</sub> Radicals.*  
436 J. Phys. Chem. A 108, 7393 – 7398, 2004  
437  
438 Feilberg, K. L., D'Anna, B., Johnson, M. S., Nielsen, C. J.  
439 *Relative Tropospheric Photolysis Rates of HCHO, H<sup>13</sup>CHO, HCH<sup>18</sup>O, and DCDO Measured*  
440 *at the European Photoreactor Facility*  
441 J. Phys. Chem. 109A, 8314 – 8319, 2005  
442  
443 Feilberg, K. L., Johnson, M. S., Bacak, A., Röckmann, T., Nielsen, C. J.  
444 *Relative Tropospheric Photolysis Rates of HCHO and HCDO Measured at the European*  
445 *Photoreactor Facility*  
446 J. Phys. Chem. 111A, 9034 – 9046, 2007  
447  
448 Fu, B., B. Shepler, B. C., and Bowman, J. M.  
449 *Three-State Trajectory Surface Hopping Studies of the photodissociation dynamics of*  
450 *formaldehyde on ab initio potential energy surfaces*  
451 J. Am. Chem. Soc. 133, 7957 – 7968, 2011  
452  
453 Gerst, S., Quay, P.  
454 *Deuterium component of the global molecular hydrogen cycle*  
455 J. Geophys. Res., 106, 5021 – 5031, 2001  
456

457 Gratien, A., Nilsson, E., Doussin, J-F., Johnson, M. S., Nielsen, C. J., Stenstrom, Y., and  
458 Picquet-Varrault, B.  
459 *UV and IR Absorption Cross-sections of HCHO, HCDO, and DCDO*  
460 *J. Phys. Chem.*, 111A, 11506 – 11513, 2007  
461  
462 Hirschfelder, J. O., Curtiss, C. F., and Bird, R. B.  
463 *Molecular Theory of Gases and Liquids*  
464 Wiley, London, 1249pp., 1954  
465  
466 Keller-Rudek, H., G. Moortgat, G. K., Sander, R., and Sørensen, R.  
467 *MPI-Mainz UV-VIS Spectral Atlas of Gaseous Molecules*  
468 <http://www.atmosphere.mpg.de/enid/2295>  
469 Last access 01.06.2022  
470  
471 Mar, K. A., McCarthy, M. C., Connell, P., K. Boering, K. A.  
472 *Modelling the photochemical origins of the extreme deuterium enrichment in stratospheric H<sub>2</sub>*  
473 *J. Geophys. Res.* 112, D19302, doi: 10.1029/2006JD007403, 2007  
474  
475 McCarthy, M. C., K. Boering, A., Rahn, T., J. Eiler, J. M., Rice, A. L., Tyler, S. C.,  
476 Schaufli, S., Atlas, E., D. Johnson, D. G.  
477 *The hydrogen isotopic composition of water vapor entering the stratosphere inferred from*  
478 *high-precision measurements of  $\delta D-CH_4$  and  $\delta D-H_2$*   
479 *J. Geophys. Res.* 109, D07304, doi:10.1029/2003JD004003, 2004  
480  
481 McQuigg, R. D., Calvert, J. G.  
482 *The Photodecomposition of CH<sub>2</sub>O, CD<sub>2</sub>O, CHDO, and CH<sub>2</sub>O-CD<sub>2</sub>O Mixtures at Xenon Flash*  
483 *Lamp Intensities*  
484 *J. Am. Chem. Soc.* 91, 1590 – 1599, 1969  
485  
486 Miller, R. G. and Lee, E. K. C.  
487 *Single vibronic level photochemistry of formaldehydes in the A <sup>1</sup>A<sub>2</sub> state: Radiative and*  
488 *nonradiative processes in H<sub>2</sub>CO, HDCO, and D<sub>2</sub>CO*  
489 *J. Chem. Phys.* 68, 4448 – 4464, 1978  
490  
491 Nelder, J. A. , and Mead, R.  
492 *A simplex method for function minimization*  
493 *Computer Journal*, 7, 308 -313, 1965  
494  
495 Nilsson, E. J. K., Bache-Andreassen, L., Johnston, M. S., and Nielsen, C. J.  
496 *Relative Tropospheric Photolysis Rates of Acetaldehyde and Formaldehyde Isotopologues*  
497 *Measured at the European Photoreactor Facility*  
498 *J. Phys. Chem.* 113A, 3498 – 3504, 2009  
499  
500 Nilsson, E. J. K., Andersen, V. F., Skov, H., and Johnson, M. S.  
501 *Pressure dependence of the deuterium isotope effect in the photolysis of formaldehyde by*  
502 *ultraviolet light*  
503 *Atmos. Chem. Phys.* 10, 3455 – 3463, 2010  
504  
505 Nilsson, E. J. K., Schmidt, J. A., and Johnson, M. S.  
506 *Pressure dependent isotopic fractionation in the photolysis of formaldehyde-d<sub>2</sub>*  
507 *Atmos. Chem. Phys.* 14, 551 – 558. 2014

508  
509 Osborn, D.L.  
510 *Exploring multiple reaction paths to a single product channel*  
511 *Adv. Chem. Phys.* 138, 213 – 265, 2008  
512  
513 Pieterse, G., Krol, M. C., Batenburg, A. M., Steele, L. P., Krummel, P. B., Langenfels, R. I.,  
514 and Röckmann, T.  
515 *Global modelling of H<sub>2</sub> mixing ratios and isotopic compositions with the TM5 model*  
516 *Atmos. Chem: Phys.*, 11, 7001 – 7026, 2011  
517  
518 Rahn, T., Eiler, J. M., Boering, K. A., Wennberg, P. O., McCarthy, M. C., Tyler, S.,  
519 Schaufli, S., Donnelly, S., Arlas, E.  
520 *Extreme deuterium enrichment in stratospheric hydrogen and the global atmospheric budget*  
521 *of H<sub>2</sub>*  
522 *Nature* 424, 918 – 921, 2003  
523  
524 Rhee, T. S., Brenninkmeijer, C. A. M., Braß, M., Brühl, C.  
525 *Isotopic composition of H<sub>2</sub> from CH<sub>4</sub> oxidation in the stratosphere and the troposphere*  
526 *J. Geophys. Res.* 111, D23303, doi:10.1029/2005JD00670, 2006  
527  
528 Rhee, T. S., Brenninkmeijer, C. A. M., and Röckmann, T.  
529 *Hydrogen isotope fractionation in the photolysis of formaldehyde*  
530 *Atmos. Chem. Phys.* 8, 1353 – 1366, 2008  
531  
532 Röckmann, T., Rhee, T. S., Engel, A.  
533 *Heavy hydrogen in the stratosphere*  
534 *Atmos. Chem. Phys.* 3, 2015 -2023, 2003  
535  
536 Röckmann, T., Walter, S., Bohn, B., Wegener, R., Spahn, H., Brauers, T., Tillmann, R.,  
537 Schlosser, E., Koppmann, R., and Rohrer, F.  
538 *Isotope effect in the formation of H<sub>2</sub> from H<sub>2</sub>CO studied at the atmospheric Simulation*  
539 *chamber SAPHIR*  
540 *Atmos. Chem. Phys.* 10, 5343 – 5357, 2010  
541  
542 Röth, E.-P.  
543 *Description of the Anisotropic Radiation Transfer Model ART to Determine*  
544 *Photodissociation Coefficients*  
545 *Ber. Forschungszentrum Jülich, Jül-3960*, 2002  
546  
547 Röth, E.-P. and Ehhalt, D. H.  
548 *A simple formulation of the CH<sub>2</sub>O photolysis quantum yields*  
549 *Atmos. Chem. Phys.* 15, 7195 – 7202, 2015  
550  
551 Troe, J.  
552 *Specific rate constants k(E,J) for the unimolecular dissociations of H<sub>2</sub>CO and D<sub>2</sub>CO*  
553 *J. Phys. Chem.*, 88, 4375 – 4380, 1984  
554  
555 Troe, J.  
556 *Analysis of quantum yields for the photolysis of formaldehyde at > 310 nm*  
557 *J. Phys. Chem. A* 111, 3868 – 3874, 2007  
558

559 Yamaguchi, Y., Wesolowski, S., Van Huis, T. J., and Schaefer III, H. F.  
560 *The unimolecular dissociation of H<sub>2</sub>O on the lowest triplet potential-energy surface*  
561 J. Chem. Phys. 108, 5281 – 5288, 1998  
562  
563 Yeung, E.S. and Moore, C. B.  
564 *Photochemistry of single vibronic levels of formaldehyde*  
565 J. Chem. Phys. 58, 3988 – 3998, 1973  
566  
567  
568

## 569 **Figures**

570

571 **Fig01** : Comparison of the fluorescence quantum yield measured by Miller and Lee (1978)  
572 (full dots) with the fitted function  $\Phi_F(M)$  (see Eq. F3) for different wavelengths in nm as  
573 indicated. To emphasize the quality of the fit, we depict only the pressure dependent part  
574  $\theta(M)$  as defined in Eq. F4

575

576 **Fig02** : The pressure dependence of the kinetic isotope effect KIE (i.e. the ratio of the  
577  $\text{CH}_2\text{O}/\text{CHDO}$  photolysis frequencies, see Eq. F6) is compared to the measured data of Nilsson  
578 et al., 2010 (blue squares), and to Feilberg et al., 2007, Rhee et al., 2008, and Röckmann et al.,  
579 2010 (red squares, 'others'). The solid curve at 1000 hPa is included to accommodate the  
580 variation of the data.

581

582 **Fig03**: The total product quantum yields  $\Phi^{\text{tot}}$  derived from the measured rate constants of  
583 Miller and Lee (1978) at 1000 hPa through Eq. F7 (full circles) is well reproduced by the  
584 continuous  $\Phi^{\text{tot}}$  function obtained after fitting the rate coefficients to function Eq. F8 (solid  
585 curve).

586 **Fig04**: Wavelength dependence of the contributions of the three terms for  $\Phi_2^{\text{tot}}$ ,  $\Phi_3^{\text{tot}}$  and  
587  $\Phi_6^{\text{tot}}$  of equation F7 to the total quantum yield  $\Phi^{\text{tot}}$  of the CHDO photolysis at 10 hPa (a) and  
588 1030 hPa (b).

589

590 **Fig05**: The total quantum yields  $\Phi^{\text{tot}}$  of the photolysis of CHDO and that of the radical  
591 channel,  $\Phi^{\text{rad}}$ , calculated with the three-term functions Eq. F7 and F10 (black curves). The  
592 blue shaded area indicates the variation of parameter  $a$  within the interval  $[0.70 / 0.78]$ . The  
593 red curves, derived using the one-term approximation (eq. F11), and the black curves fall  
594 within the variance of each other.

595

596 **Fig06**: Comparison of the one-termfit function F11 (open circles on the solid line) with the  
597 measured data (Miller and Lee, 1978) of the total photolytic quantum yields  $\Phi^{\text{tot}}$  (full circles)  
598 at 1, 10, 200, and 1000 hPa.

599

600 **Fig07**: The original data of McQuigg and Calvert (1969) for  $\text{CH}_2\text{O}$  (full red squares) and  
601  $\text{CD}_2\text{O}$  (open squares) for the photolytic quantum yields of the radical channel are compared to  
602 the averaged function for  $\text{CH}_2\text{O}$  by Röth and Ehhalt (2015).

603

604 **Fig08:** The ratio  $\Phi_{\text{CD}_2\text{O}}/\Phi_{\text{CH}_2\text{O}}$  of the McQuigg and Calvert (1969) data shown in Fig.7 and  
605 the corrected radical quantum yield of  $\text{CD}_2\text{O}$ ,  $\Phi_{\text{CD}_2\text{O}}^{\text{rad}}$  (black squares). The ratio of the  
606 respective reaction constants (triangles) derived theoretically by Troe (1984) shows the same  
607 tendency as the quantum yield ratio.

608

609 **Fig09:** Wavelength dependency of the quantum yields  $\Phi^{\text{rad}}$  for the radical channel of the three  
610 isotopologues of formaldehyde. The curves for  $\text{CH}_2\text{O}$  (Röth and Ehhalt, 2015) and that for  
611  $\text{CD}_2\text{O}$  (corrected data of McQuigg and Calvert, 1969) are used to calculate the quantum yield  
612 of  $\text{CHDO}$  (black dots) by their mean values.  $\Phi_{\text{CHDO}}^{\text{rad}}$  is then fitted by the one-term function Eq.  
613 F14 (black line).

614

615 **Fig10:** The  $\text{CHDO}$  quantum yield  $\Phi_{\text{CHDO}}^{\text{rad}}$  fit function deduced from the fluorescence  
616 measurements (blue line, Eq. F11) of Miller and Lee (1978), and that from the interpretation  
617 of the photo-decomposition (red line, Eq. F14) measurements of McQuigg and Calvert  
618 (1969). These lie within the uncertainty range of each other. Also depicted is the function for  
619 the total quantum yield  $\Phi^{\text{tot}}$  (Eq. F11)

620

621 **Fig11 :** The photolysis rate is the combination of the actinic photon flux, the absorption cross  
622 section and the quantum yield. Depicted are the contributions to the molecular channel of the  
623 photolysis rate of  $\text{CHDO}$ ,  $J_{\text{CHDO}}^{\text{mol}}$ , at 20 km altitude and integrated over 5 nm wavelength: the  
624 actinic photon flux  $F_{\lambda}(\lambda)$ , the absorption cross section  $\sigma(\lambda)$  (Gratien et al., 2007), and the  
625 quantum yield for the molecular channel  $\Phi^{\text{mol}}(\lambda)$ . The photolysis rate, the photon flux and the  
626 cross section are multiplied by  $2.5 \times 10^5 \text{ sec}$ ,  $2.5 \times 10^{-15} \text{ photons}^{-1} \text{ nm sec}$ , and  $1.5 \times 10^{19} \text{ cm}^{-1}$ ,  
627 respectively, to achieve comparability.

628

629 **Fig12 :** The altitudinal dependence of the photolysis frequencies  $J_{\text{mol}}$  of the molecular  
630 channels (a) of  $\text{CH}_2\text{O}$  and  $\text{CHDO}$  is important for the atmospheric production of HD. For  
631 comparison the radical channels (b) are also depicted. The dependence on altitude of the  
632 kinetic isotope effect,  $\text{KIE} = J_{\text{CH}_2\text{O}}/J_{\text{CHDO}}$ , is more pronounced for the molecular channel than  
633 the radical channel. The shaded area indicates the variance upon changing (a) the quantum  
634 yield  $\Phi^{\text{mol}}$  by 10% and (b) the radical threshold wavelength by 3 nm.

635

636 **Fig13 :** At 50 km altitude the solar zenith angle dependency of the photolysis frequency ratio  
637 of the molecular channel is nearly constant. In contrast, at 0 km the ratio increases  
638 significantly for solar zenith angles above 30 degrees.  
639  
640  
641

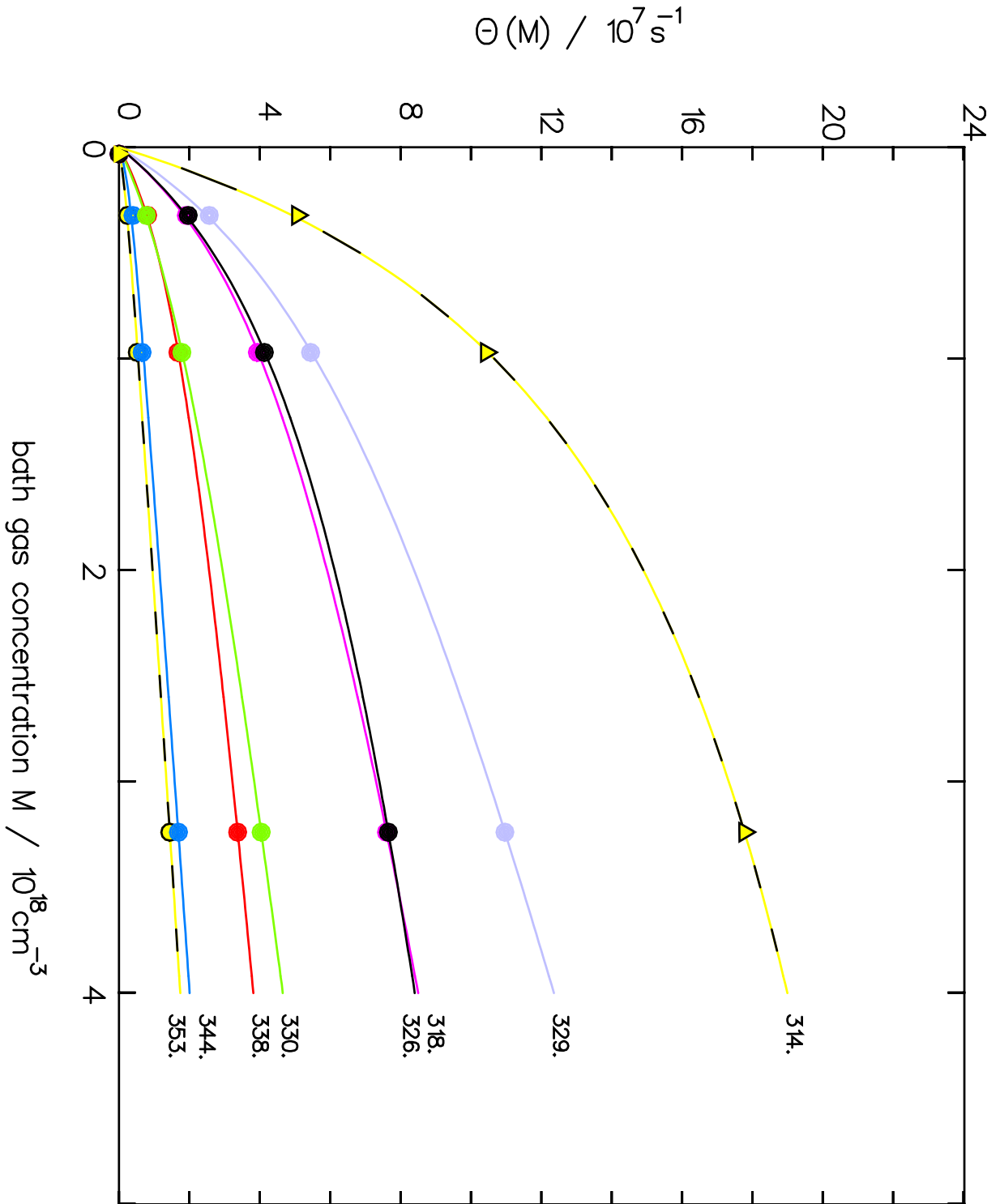


Fig. 1

642  
643  
644  
645  
646  
647

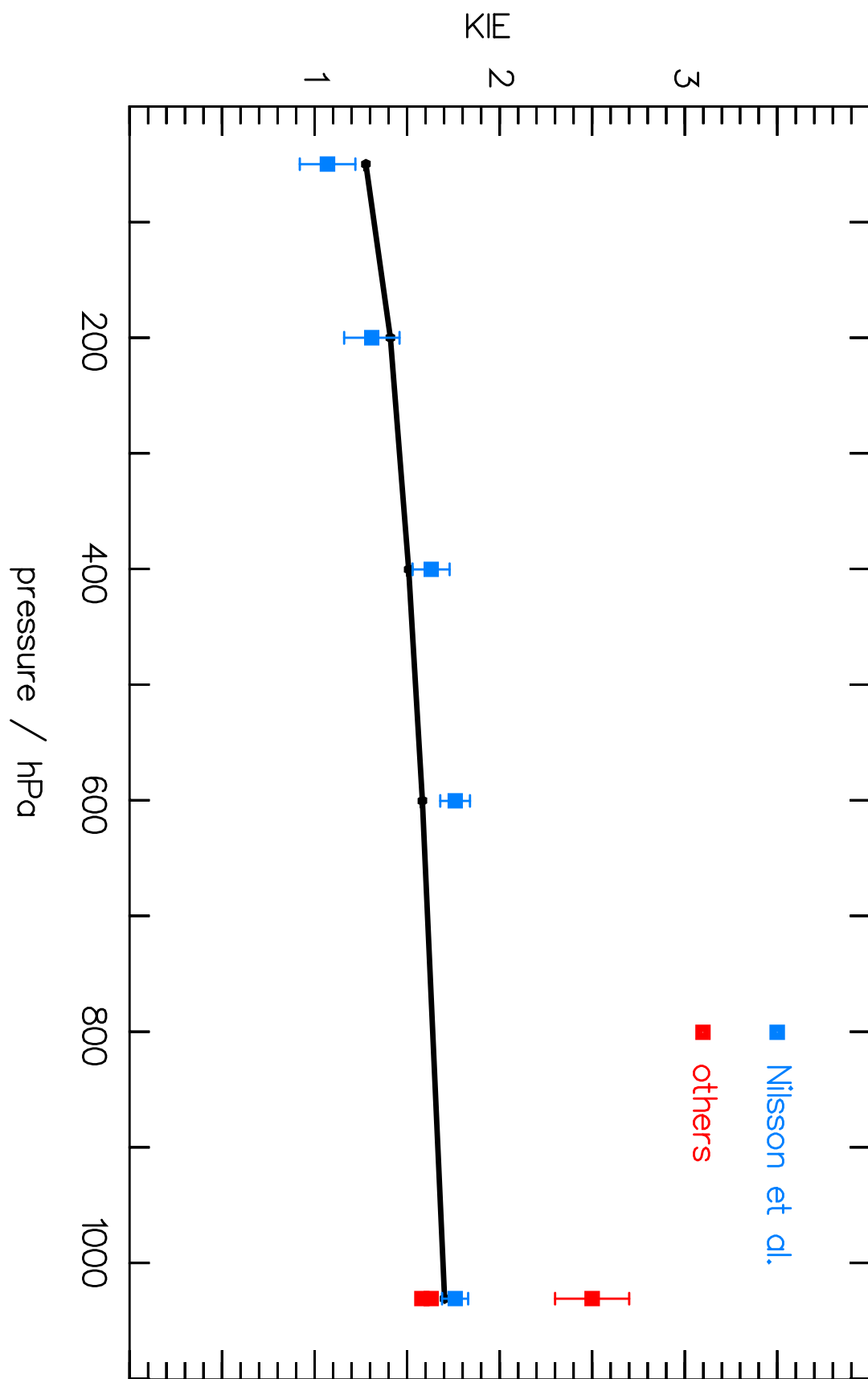


Fig. 2

648  
649  
650  
651

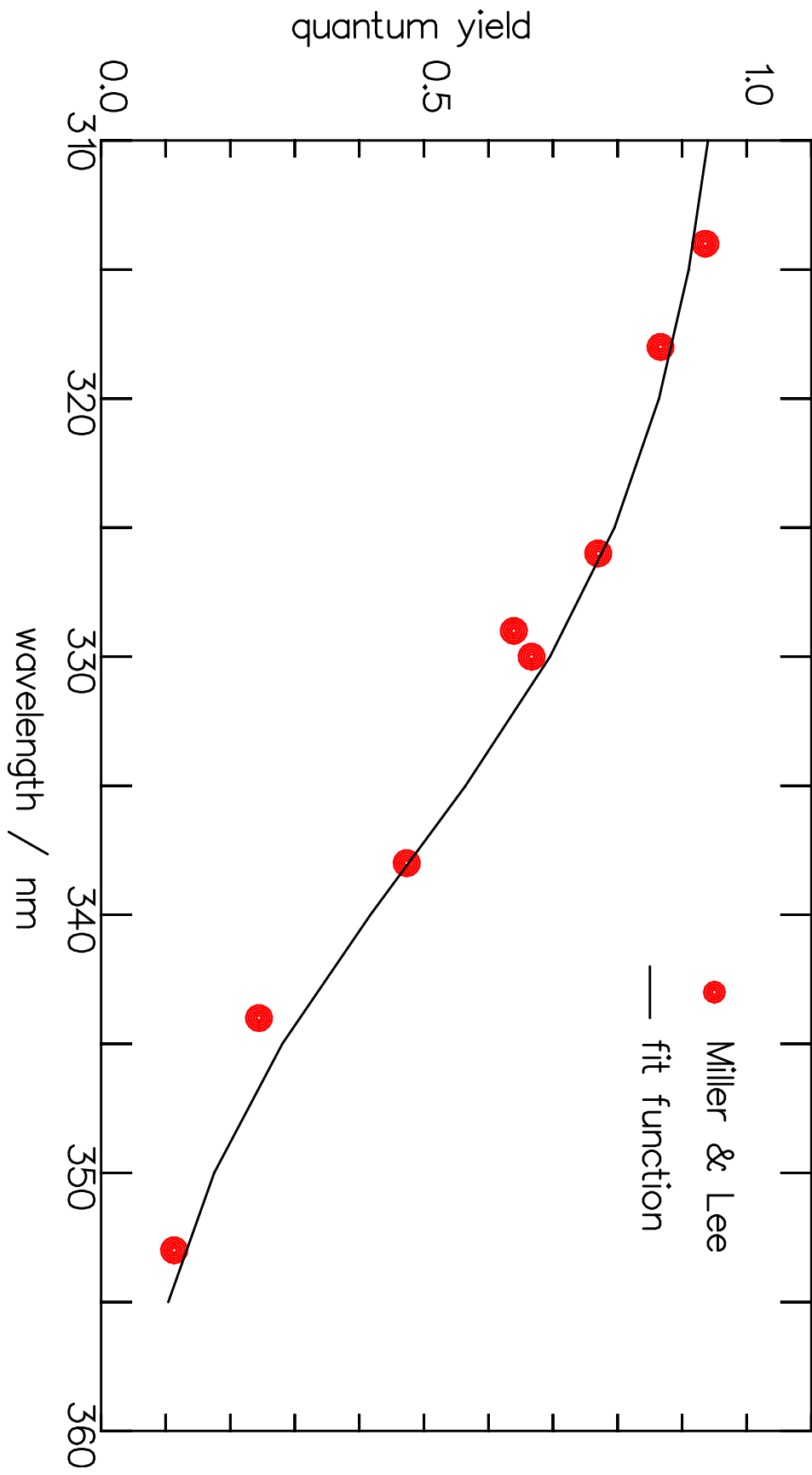


Fig. 3

652  
653  
654  
655

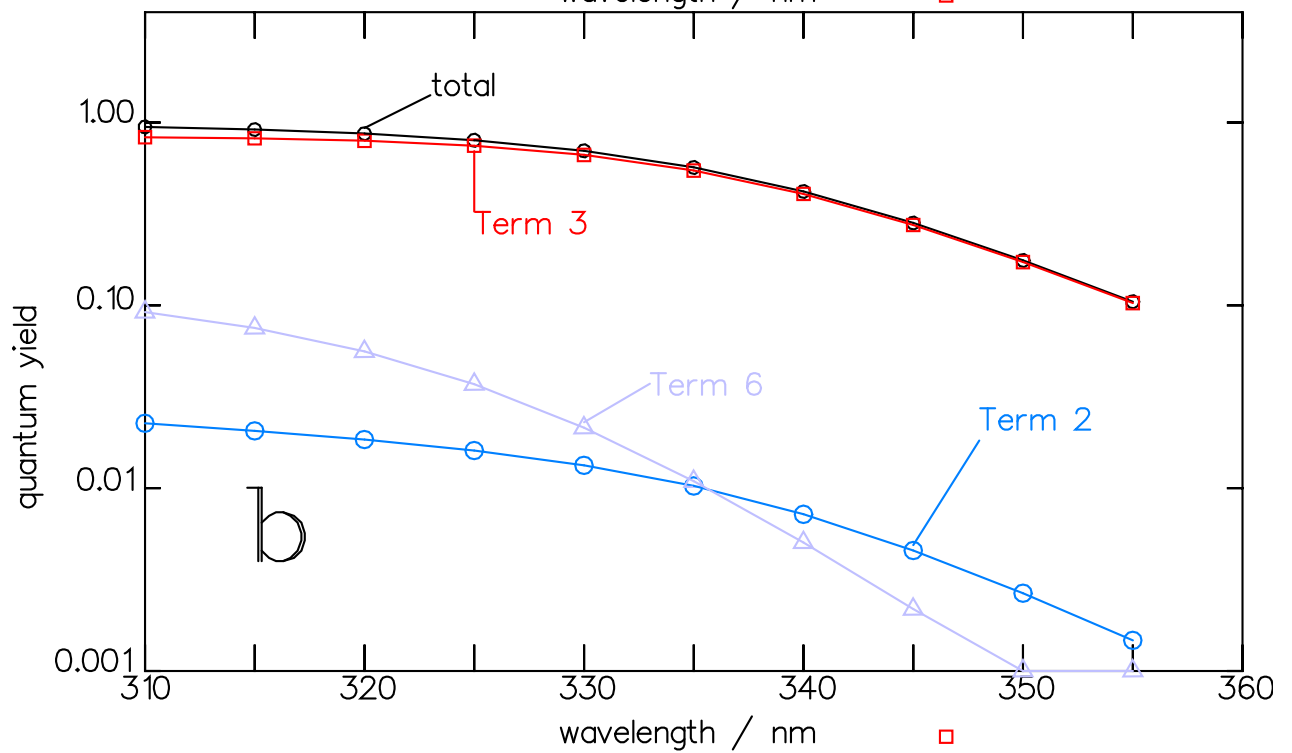
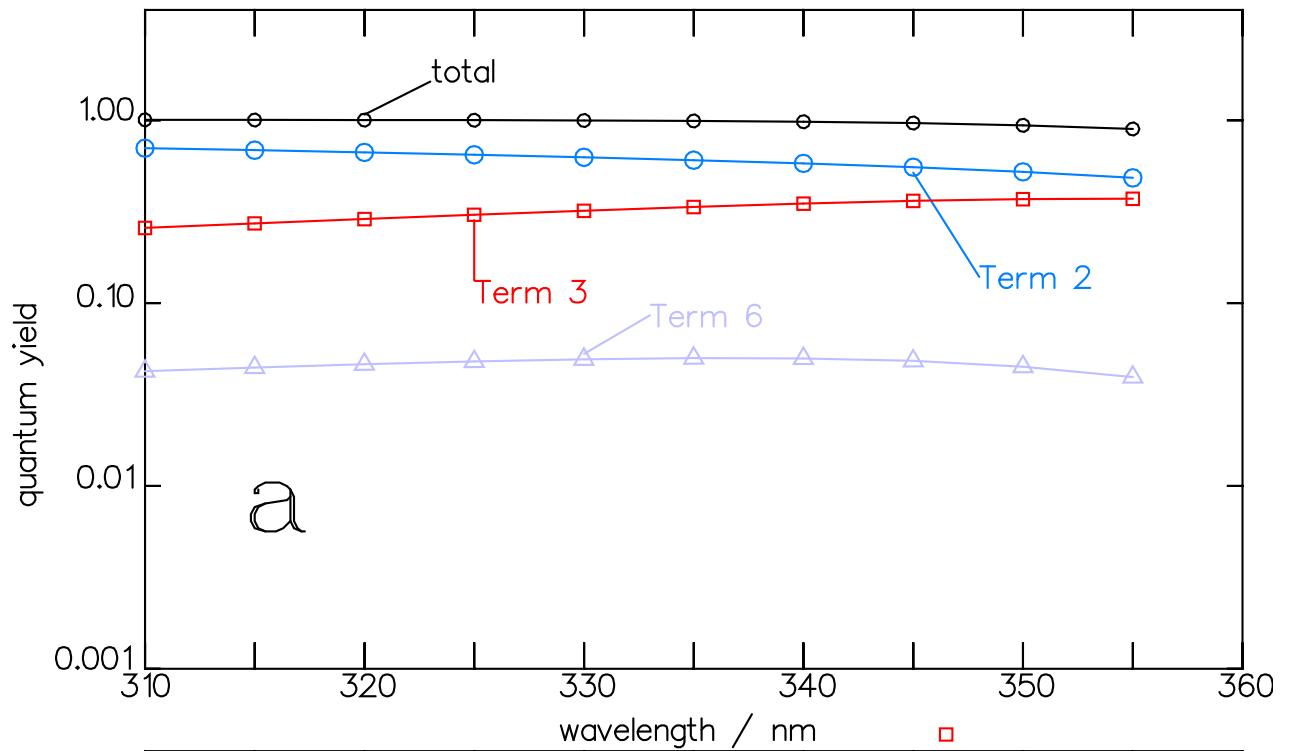


Fig. 4

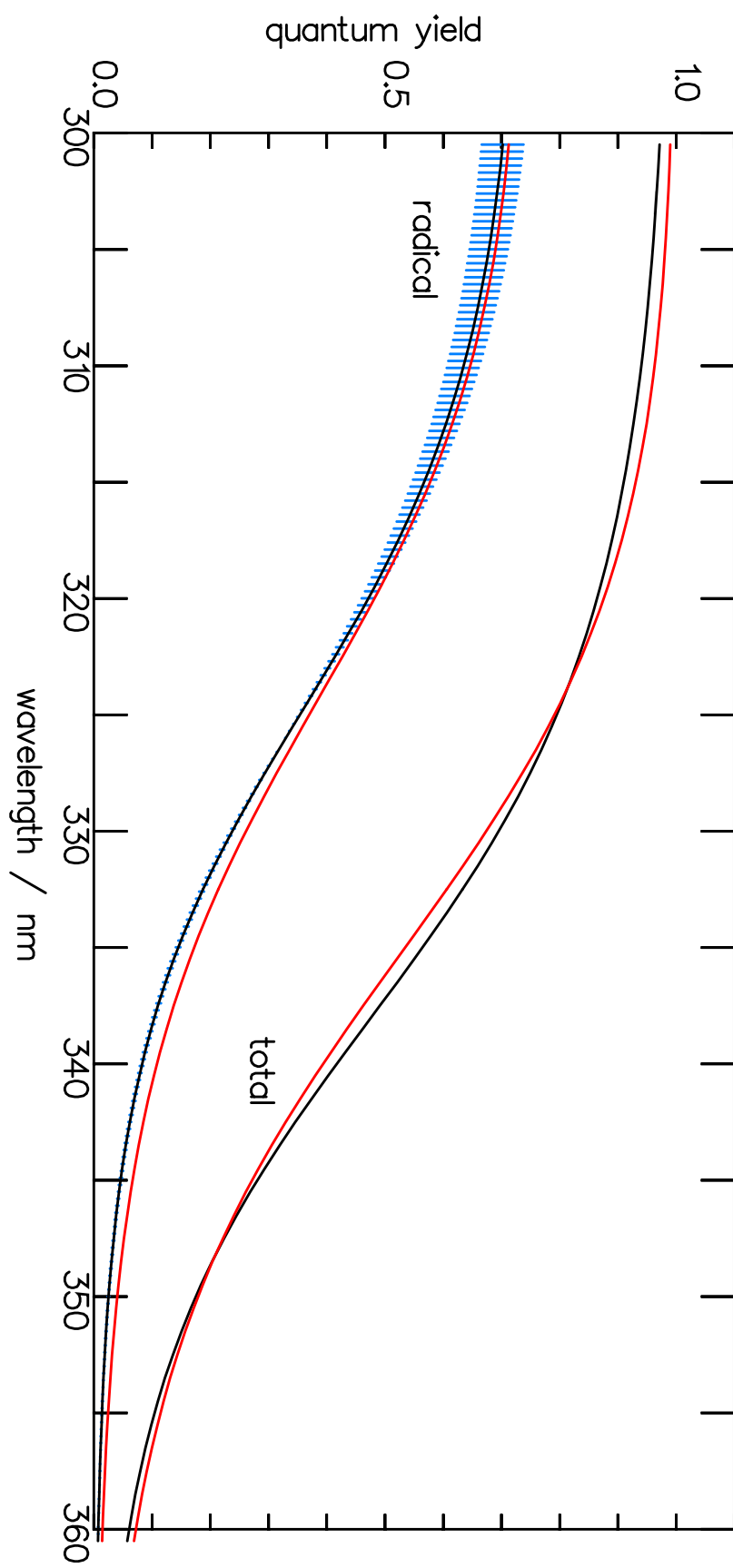


Fig. 5

661  
662  
663  
664

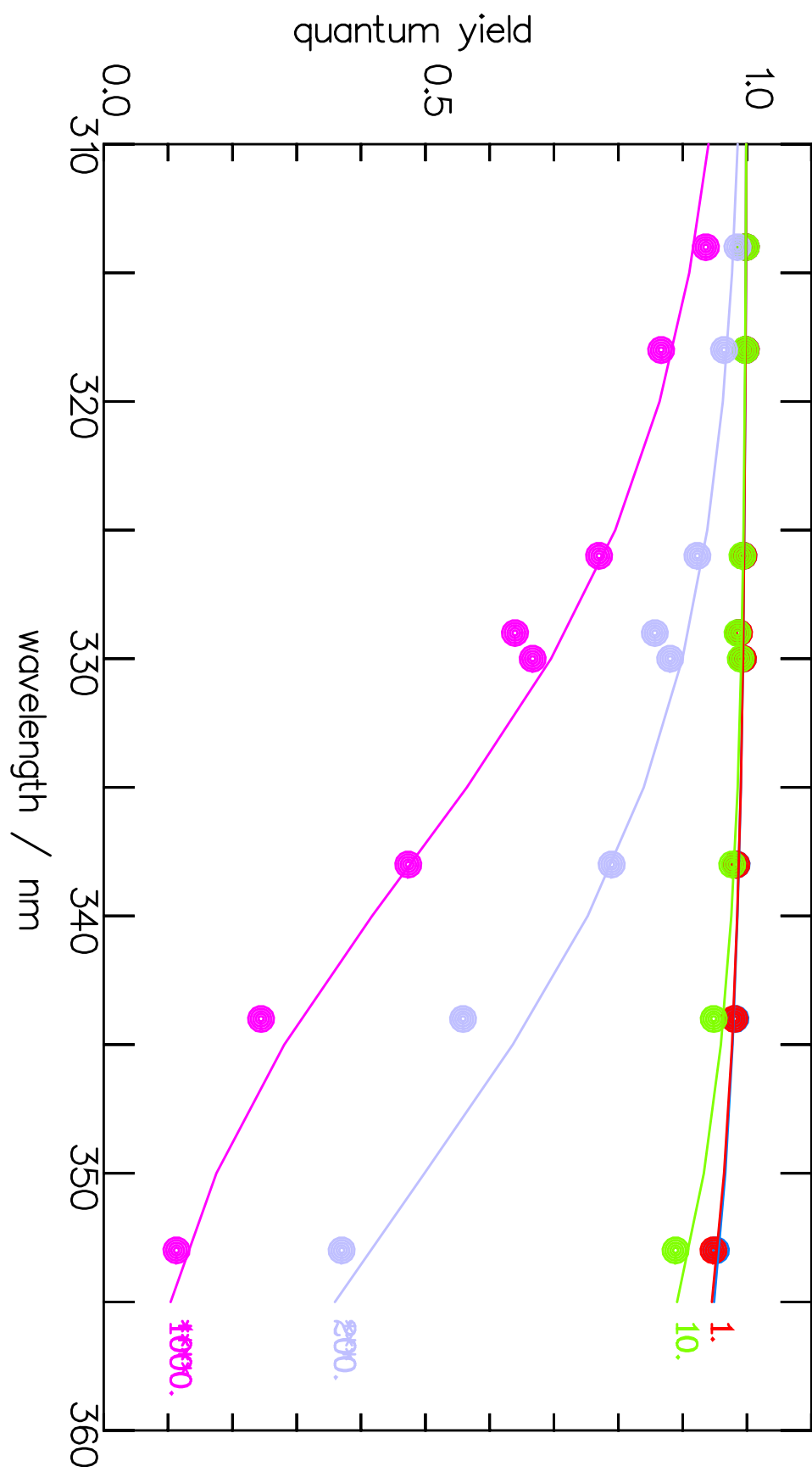


Fig. 6

665  
666  
667  
668

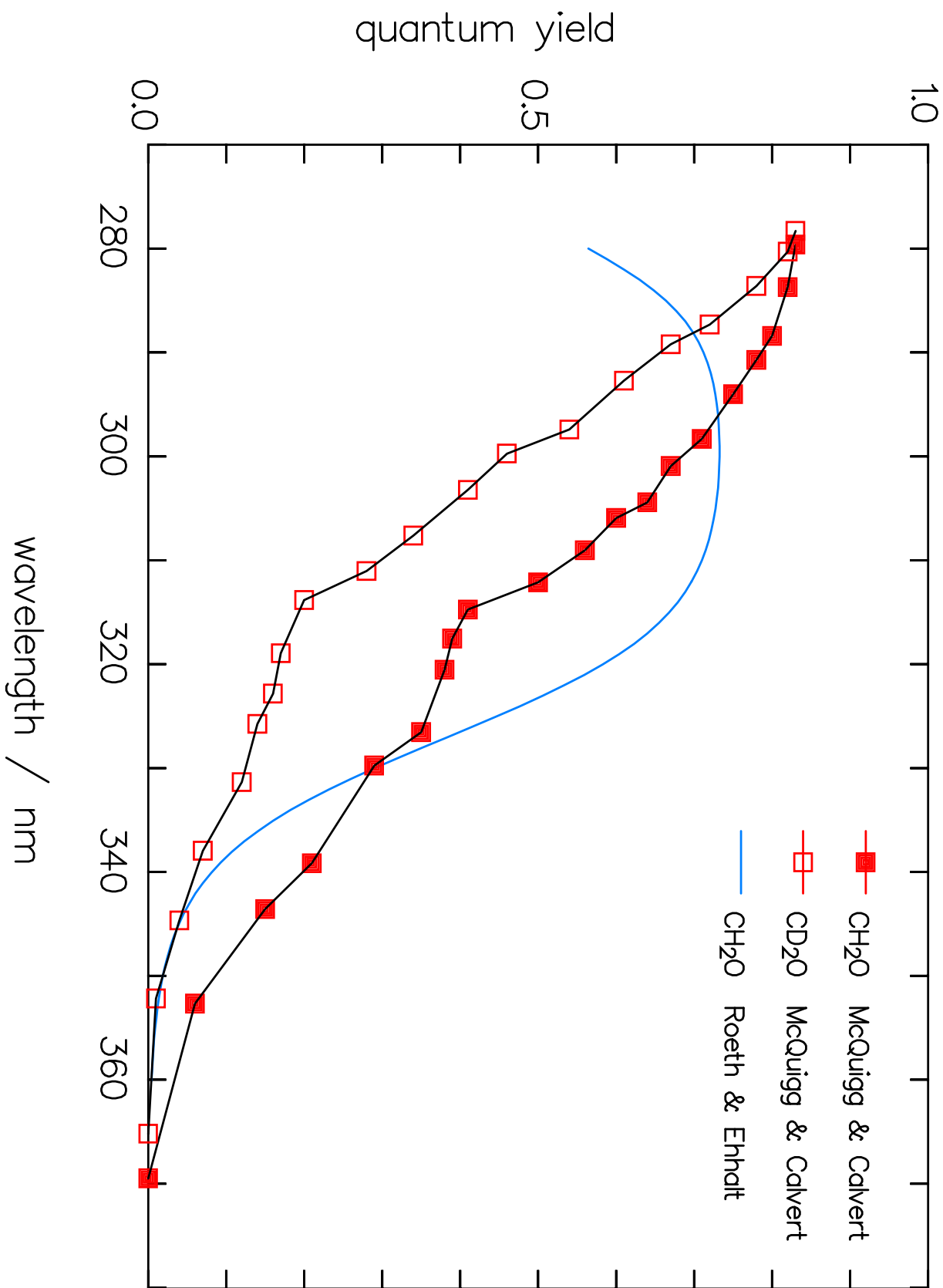


Fig 7

669  
670  
671  
672

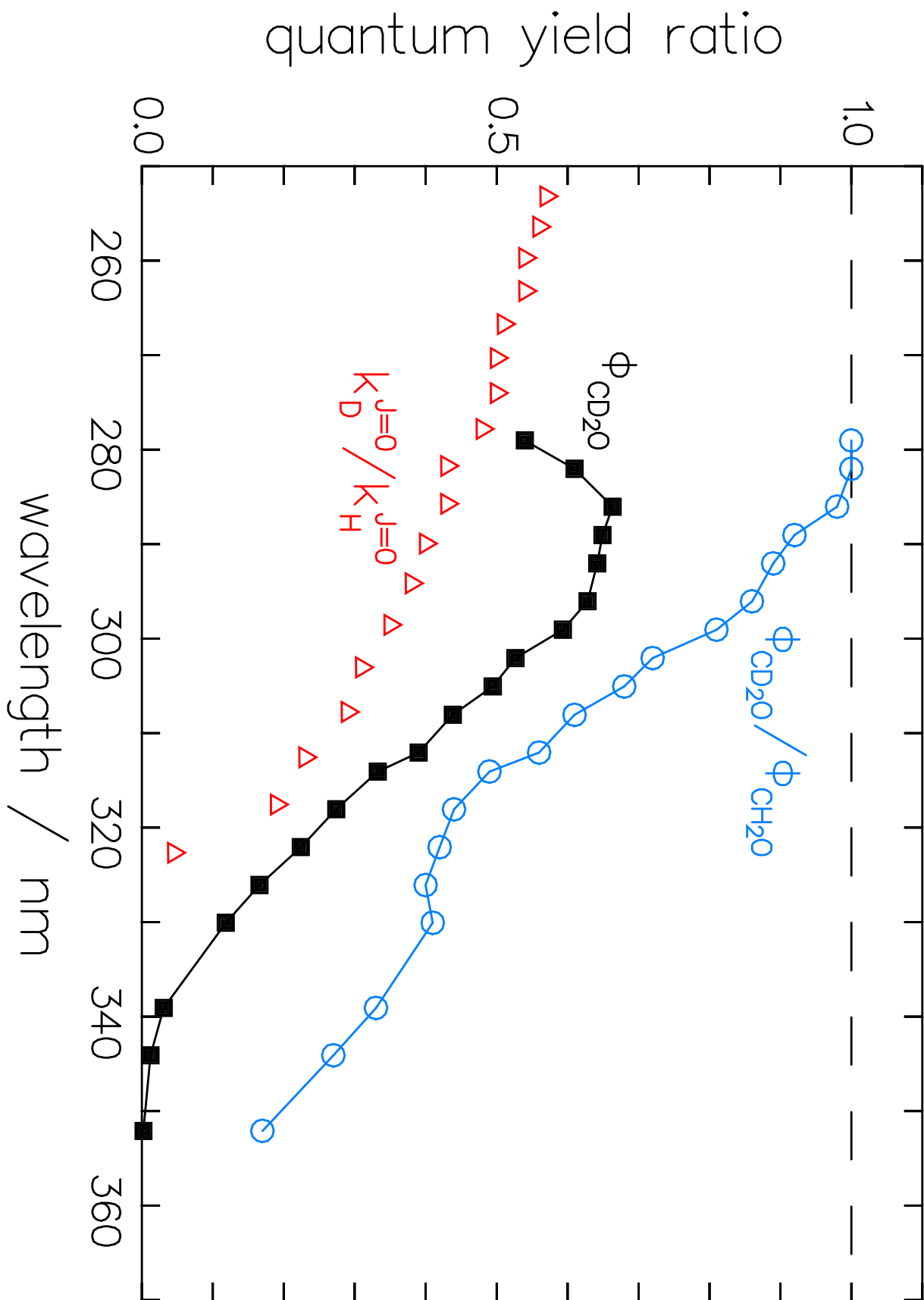


Fig. 8

673  
674  
675  
676

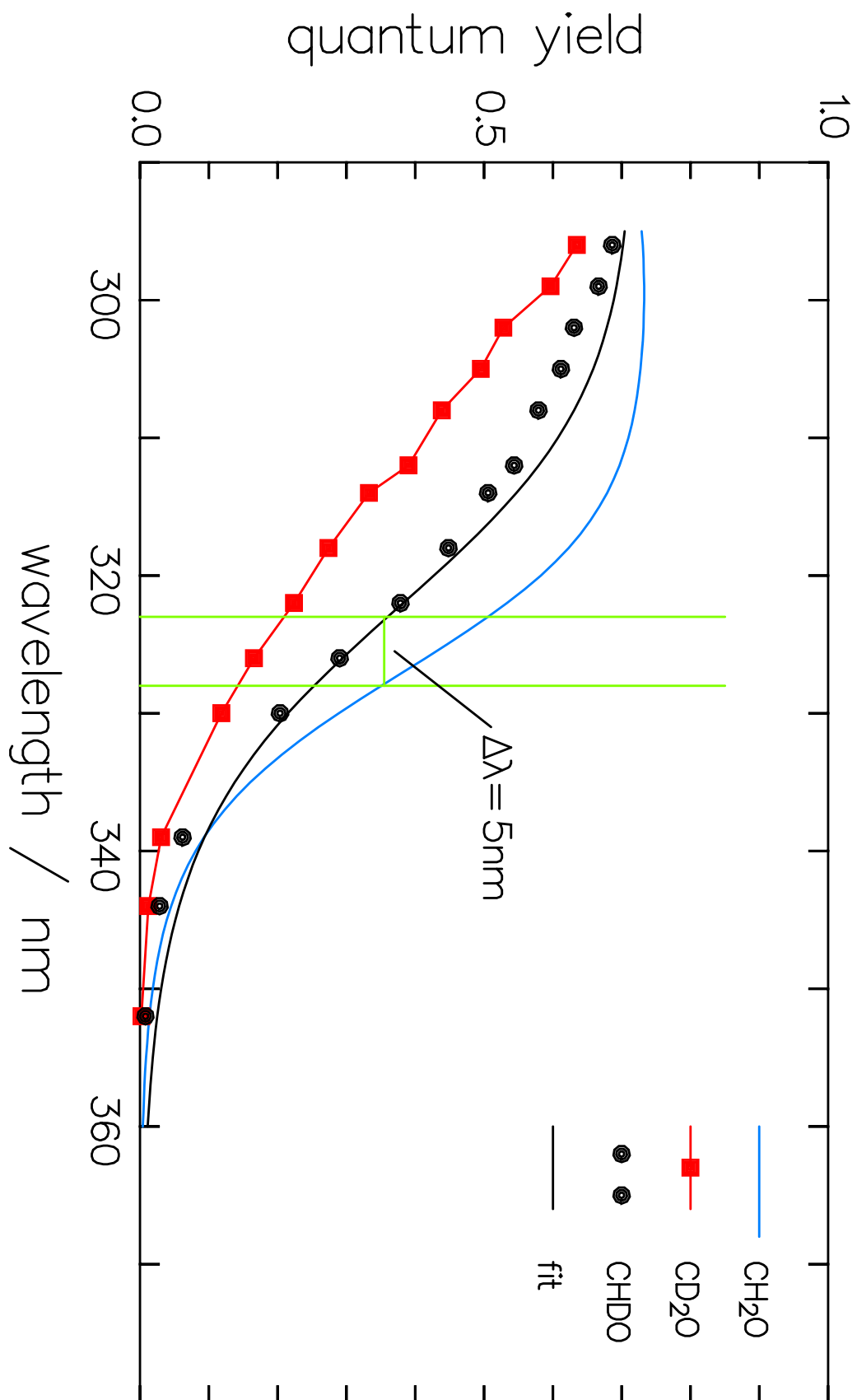


Fig. 9

677  
678  
679  
680

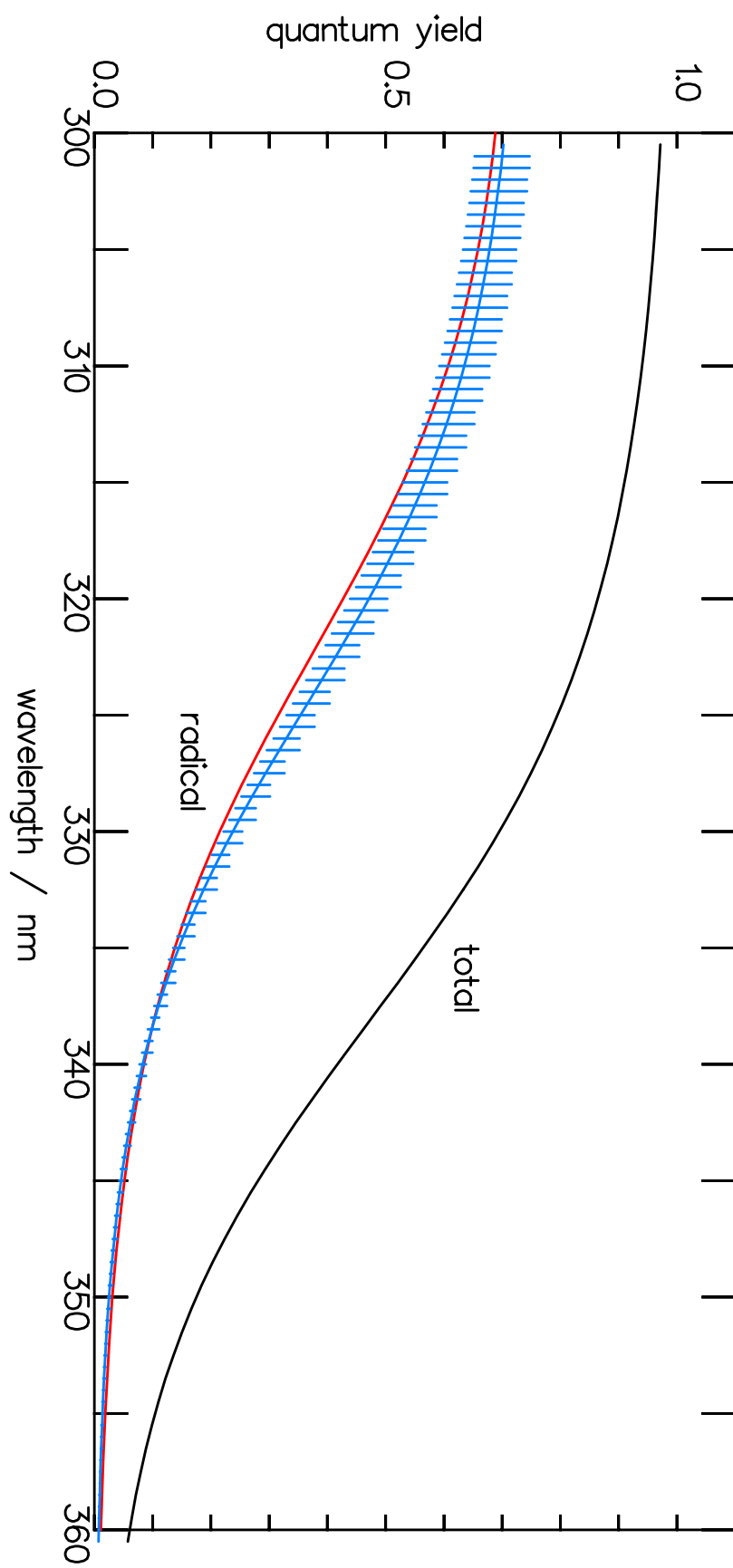


Fig. 10

681  
682  
683  
684

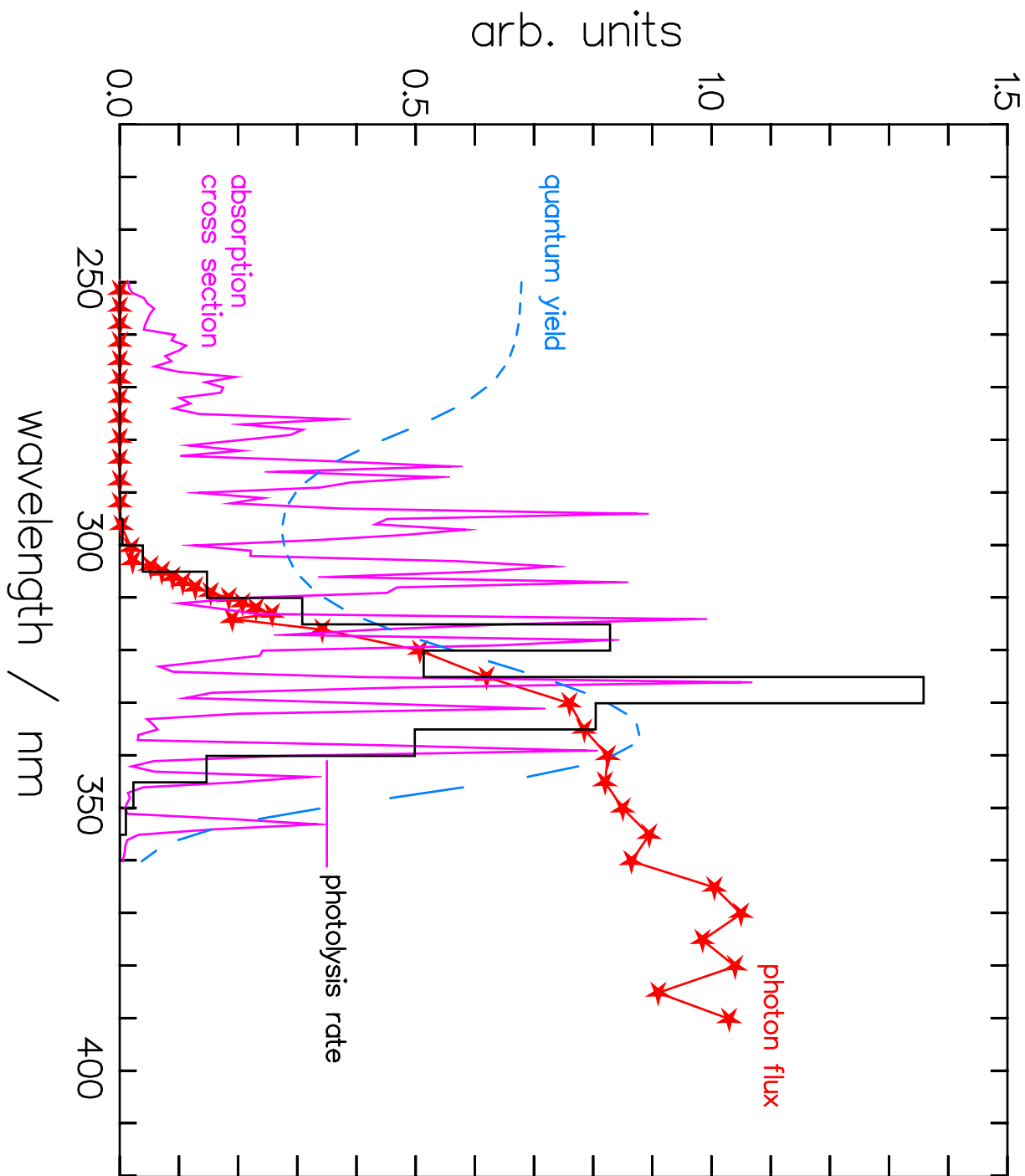
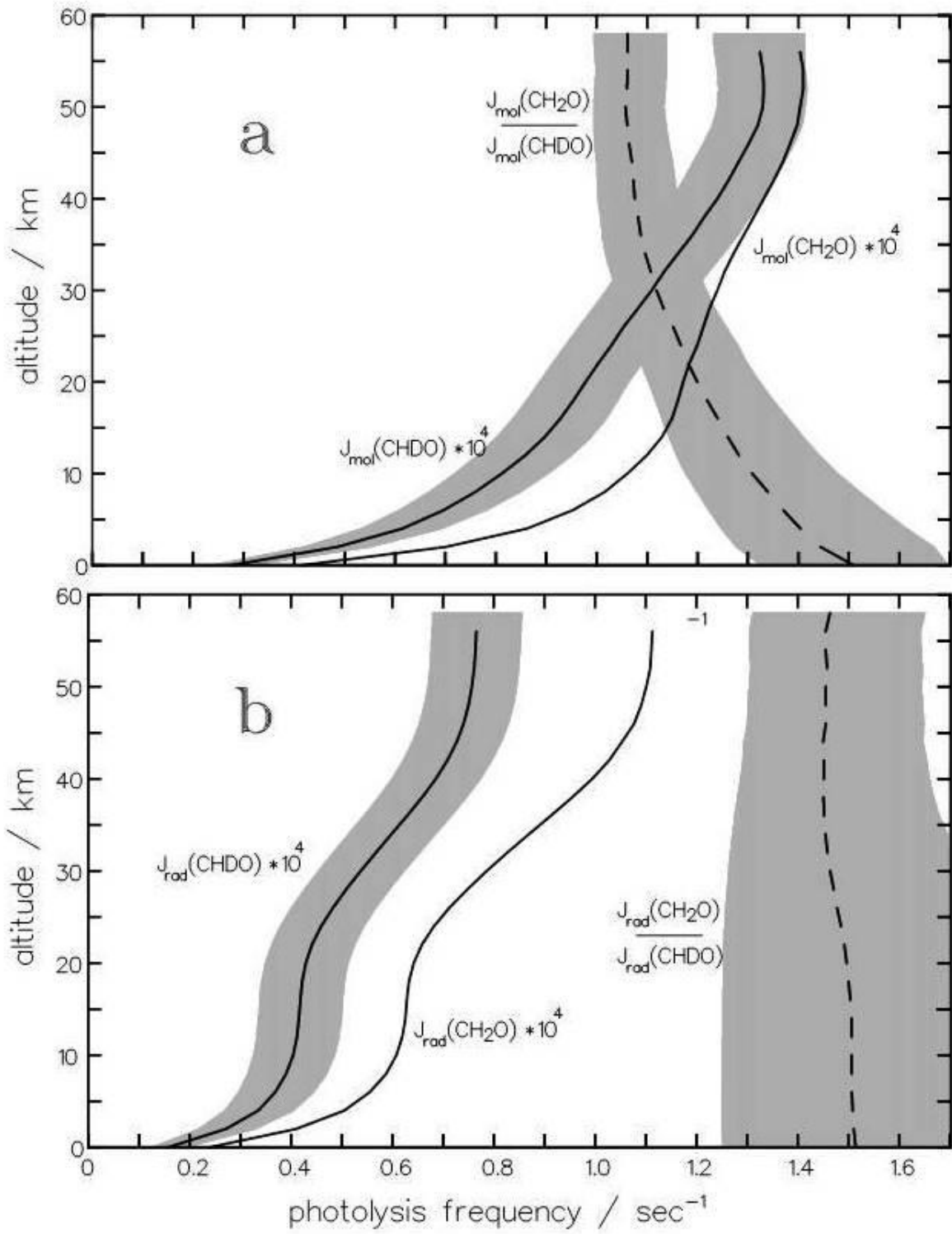


Fig. 11

685  
686  
687  
688  
689  
690



692

693

694

695

696

Fig. 12

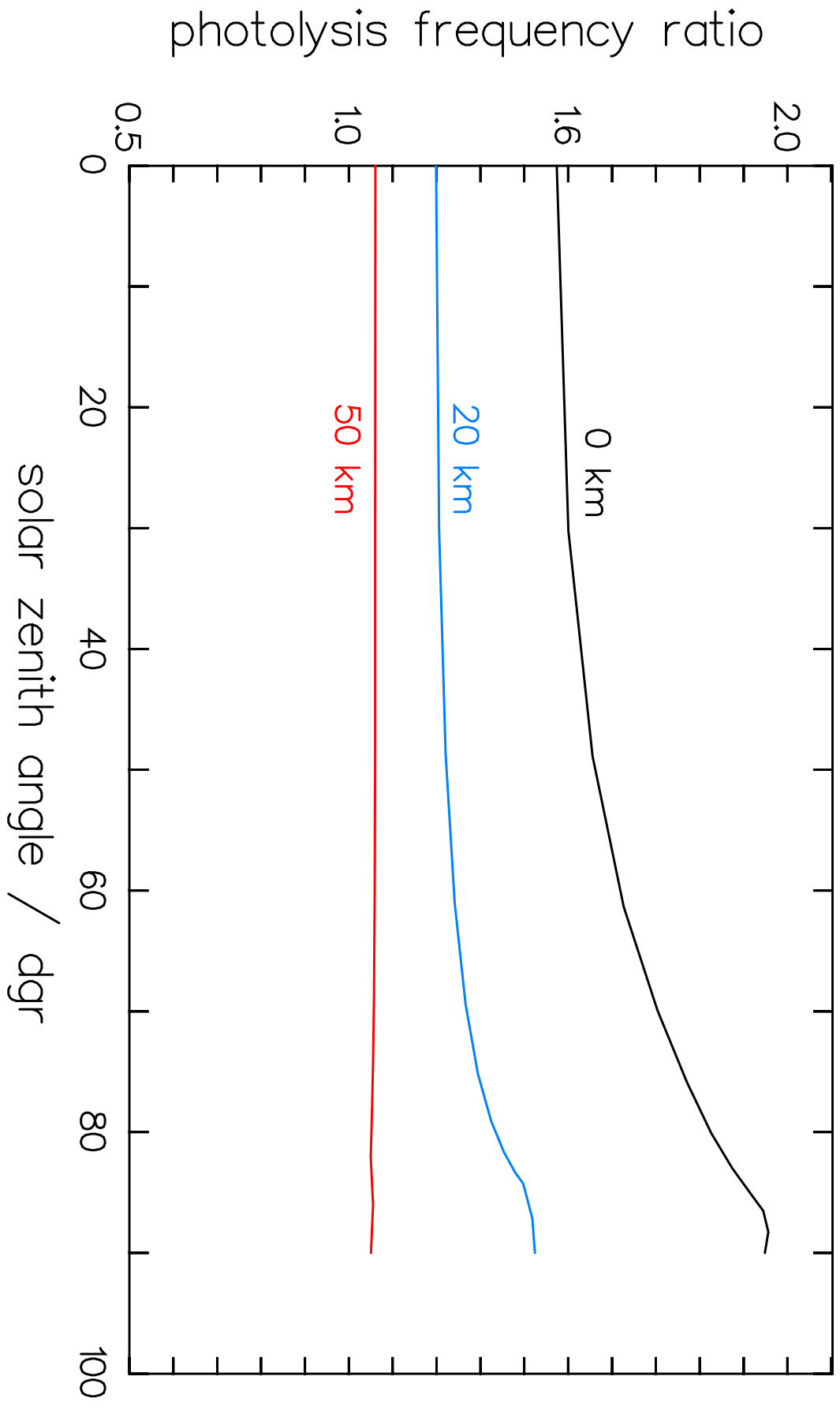
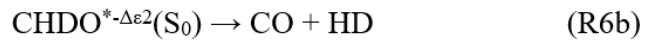
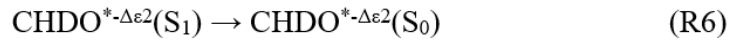
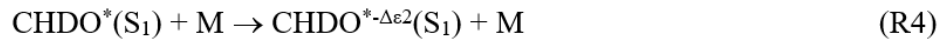
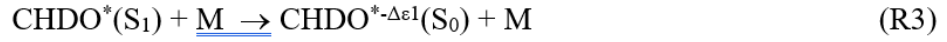


Fig. 13

697  
698  
699

700



701

702

703

## Reaction scheme (Table 1)